

Probing Dark Matter-Electron Interactions in the Cosmic Microwave Background Radiation

Rahul Dhyani,^{a,1} Arnab Paul,^{b,1} Arindam Chatterjee^{a,2}

^aDepartment of Physics, Shiv Nadar Institution of Eminence Deemed to be University, Gautam Buddha Nagar, Uttar Pradesh 201314, India

^bCentre for Strings, Gravitation and Cosmology, Department of Physics, Indian Institute of Technology Madras, Chennai 600036, India

E-mail: rahul.physics123@gmail.com, arnabpaul9292@gmail.com,
arindam.chatterjee@snu.edu.in

Abstract. In this article, we consider Dark Matter (DM) interactions, and study the same in the light of the Cosmic Microwave Background Radiation (CMBR) data. In particular, we focus on the DM-electron interactions. Assuming that such interactions are mediated by rather heavy mediators, we consider effective operators describing the relevant interaction terms in the lagrangian. The presence of such interaction terms lead to both DM annihilation and DM-electron scattering (drag). We focus on operators which lead to velocity-independent DM annihilation and DM-electron scattering cross-sections. Using the CMBR data, we study the the implications of both of these effects imposing constraints on the respective effective operators. This analysis underscores the importance of taking both scattering and annihilation processes into consideration in the study of DM interactions. We observe that the constraints on the DM annihilation and scattering cross-sections can change, up to about 14% and 13% respectively, for the benchmark scenarios we considered, depending on the mass of DM, as compared to the scenario where only DM annihilation is accounted for.

Contents

1	Introduction	2
2	DM Interactions with the SM: Implications in the light of CMBR	4
2.1	DM Annihilation into $\bar{e}e$	4
2.2	DM scattering with SM	7
2.2.1	Cosmological perturbations with DM - e scattering	8
3	DM-electron Interaction: An Effective Operator Approach	10
4	Results	11
4.1	Likelihood analysis and Constraints of Cosmological Parameters	12
4.1.1	Comment on S_8 or σ_8 Tension	18
4.2	Constraints on lagrangian Parameters	19
5	Conclusions	20
A	The Collisional Boltzmann Equation	22
A.1	Momentum transfer for DM-electron scattering	23
A.2	Drag from DM-Electron Scattering	23
B	Cross-section for Annihilation and Scattering	26

Contents

1 Introduction

The standard model of cosmology, the Λ CDM model, has been successful in the light of various observational data, including the anisotropy of the Cosmic Microwave Background (CMBR) [1, 2]. In the simplest version, this model incorporates cosmological constant Λ and Cold Dark Matter (CDM) species; which does not interact with the constituent particles of the Standard Model (SM) of particle physics. It is estimated that CDM and Λ account for approximately 26% and 69% [2] of the current energy budget of our Universe respectively.

While there is no suitable candidate for DM within the SM of particle physics, several well-motivated extensions of the SM incorporate particle DM candidates; see, e.g. refs. [3–5] for reviews. In most theoretical frameworks, DM possesses non-vanishing interactions with the SM particles. For instance, Weakly Interacting Massive Particles (WIMP), which have been well studied in the literature as DM candidates, possess sizable interaction with the SM particles. Adequate interaction with the SM particles are essential for the thermal production of such DM candidates in the very early Universe [6].

The possibility of interactions between DM and SM particles has been widely explored in the search for DM. Both direct detection experiments [7–11] and indirect searches [5, 12–23] of DM constrain such interactions. Further, within specific theoretical frameworks, signatures of DM in the form of missing energy and momentum have been probed at high-energy colliders [24–31], which constrains the the production cross-section of DM particles, and thus, the interaction strengths of SM and DM particles. It is important to note that search for particle DM candidates in direct detection experiments can generally be challenging for rather light (sub-GeV) DM candidates, due to rather small momentum transfer to the nuclei. In this context, the interaction of DM with electrons in the heavy atoms (see e.g. [32, 33]), or in the semi-conductor materials (e.g. in silicon [34, 35]) and/or with various collective excitations have been explored in different materials, see e.g. ref. [36] for review. In particular, stringent constraints on DM-electron interaction for rather light DM from the direct searches [34, 35, 37] have been obtained.¹

In the era of precision cosmology, cosmological data has been used in the literature to probe and constrain DM interactions. In particular, the effect of DM annihilation [44–53] and scattering with the baryonic matter (and electrons) [54–65] on the CMBR anisotropy has been well studied in the literature. To be specific, DM annihilation into visible matter during and around the recombination epoch can lead to ionization and excitation of the neutral hydrogen atoms, and heating of the baryonic plasma. This can enhance the duration of the recombination epoch. Further, DM annihilation can lead to an enhanced electron-positron number density around the same epoch; which affects the polarization of CMBR photons. Apart from this, DM annihilation can leave its imprint on the CMBR spectral distortion as well [66–68]. The scattering of SM particles, in particular, protons, neutrons (which are in the helium atoms) and electrons, around the recombination epoch also leaves its imprint in the CMBR, as such processes affect the evolution of perturbation. The scattering process leads to cooling of the baryon temperature, and it washes out power in the small length scales. This, in turn, has been used to constrain such scattering or “drag” processes. Apart from interactions with the visible particles, interactions between DM with neutrinos [69–73], Dark Radiation (DR) [74] and Dark Energy (DE) [75, 76] have been studied in different contexts in the light of CMBR data. Note that, during the recombination epoch, the evolution of density, as well

¹Note that, for DM to reach the detectors, its interaction with SM particles should be sufficiently weak so that it traverses through Earth’s atmosphere and the experimental shielding [8, 38–43].

as the peculiar velocities are governed by (linear) perturbation theory, and thus, computation of the power spectrum involves linear calculations. This enables the detection of rather small deviations from the standard picture and is generally insensitive to uncertainties on the DM density (and velocity) profile unlike direct/indirect searches. It is worth mentioning that, the effect of DM annihilation has been studied in the context of reionization [77–84], and proposals have been made to probe the same in 21 cm cosmology [85]. Further, there have been studies on constraining annihilation of light DM from the Big Bang Nucleosynthesis (BBN) [86–90].

From the perspective of a theoretical model of particle DM, interactions with the SM particles are described by an interaction term in the lagrangian. Such interactions, if present, generally lead to both DM annihilation into a pair of SM particle and anti-particle, when the process is kinematically allowed; as well as the scattering of DM with the respective SM species. Thus, in such scenarios, it is essential to take both DM annihilation and scattering into consideration. In the present work, we consider DM interactions with electrons described by effective operators². This is appropriate when the interactions are mediated by a rather heavy mediator, the mass of which is much greater than twice the mass of the DM particle. In general, there may be different operators at play, and different operators may dominate the annihilation and the scattering processes with electrons. Further, it may also happen, depending on the interaction terms present and the mass of the DM particle, that annihilation and scattering with electrons, as well as scattering with protons (and neutrons) are present. From the perspective of the cosmological framework, thus, the relevant extension of Λ CDM includes two parameters, describing the effect of the DM scattering or drag, as well as the DM annihilation. It is important to study such a scenario, as it illustrates the properties of DM and provides complimentary constraints on the same at a very different epoch (around the recombination) in the evolution of the Universe; ii) it is useful to establish the robustness of the cosmological parameters within the base Λ CDM model and study possible degeneracies with the additional parameters³. In the present context, we study the effect of DM scattering or drag and annihilation into electrons, for scalar and fermionic DM candidates using a modified version of CLASS [100, 101]. We perform a Bayesian analysis using the publicly available package MontePython [102] to determine the upper limits on the relevant parameters using the CMBR data from Planck [2]. Using this upper limit, we constrain the effective interaction terms in the lagrangian for different masses of DM particles within the range of 1 MeV - 10 GeV. For simplicity, we have considered the presence of one interaction term at a time, while deriving the constraints on the relevant lagrangian parameters.

The paper is organized as follows. In Sec. 2, we briefly discuss the effect of DM annihilation into a pair of electron-positron, and the effect of DM scattering with electrons in the light of CMBR. We considered individual effects of annihilation and scattering in this discussion. Further, we also review the relevant perturbation equations in this context. In Sec. 3, we sketch the effective interaction terms in the lagrangian describing the DM-electron interactions in the context of a scalar and a fermionic DM. Following this, in Sec. 4 the effects of DM annihilation and scattering with electrons have been discussed on the CMBR

²Generally DM particles may interact with any SM particles, thus, effectively interacting with protons and electrons, which are present around the recombination epoch. However, for example, in the leptophilic models of DM, it interacts with only leptons, see e.g. [91].

³In the later context, it is worth noting that DM-SM particle scattering, if present, can relax the discrepancy [92, 93] in the determination of the σ_8 parameter, which arises while determining this parameter using CMBR data, as well as using data from various galaxy surveys [94–99].

temperature and the polarization power spectra. In the same section, we then present our results : the constraints on the annihilation and drag parameters from the CMBR data, and the respective constraints on the DM-electron interaction terms in the lagrangian. We have used Planck 2018 data set (Planck high-l TTTEEE lite, low-l TT, low-l EE, lensing). Finally, in Sec. 5 we conclude.

2 DM Interactions with the SM: Implications in the light of CMBR

In this section, we review the implications of DM (χ) annihilation in the early Universe in the light of CMBR. In particular, we focus on the effect of DM annihilation around the last scattering surface ($z \simeq 1100$). In presence of the interaction terms between the DM and the SM fields in the lagrangian, two DM particles can annihilate into SM particles, when such a process is kinematically viable. If DM particles thermalized with the SM particles in the very early Universe, as is the case for thermally produced DM particles, the DM annihilation rate becomes much smaller in comparison with the expansion rate after the thermal freeze-out. The success of the standard Big Bang Nucleosynthesis (BBN) however, constraints the mass of DM ($m_\chi \gtrsim 10$ MeV [89] for DM candidates which thermalize with the SM thermal bath. In the following discussion, we will be agnostic about the production mechanism for DM. Further, note that, for DM annihilation into a pair of electron-positron pair to be kinematically viable, the minimum mass of such a DM particle needs to be greater than about 0.5 MeV, i.e. $m_\chi \gtrsim m_e$. We will consider m_χ in the ballpark of $\mathcal{O}(1)$ MeV - $\mathcal{O}(10)$ GeV in the present context. In the following, we begin by reviewing the implications of DM annihilation into a pair of electrons and positrons in the early Universe around the epoch of recombination.

2.1 DM Annihilation into $\bar{e}e$

Around the epoch of recombination, DM annihilation into the SM particles, in particular into a pair of electron and positron, injects energy in the SM thermal bath. The thermal bath around this epoch consists of photon and mostly electrons, protons and helium nuclei. The efficiency and redshift dependence of the energy transfer process from the DM to the SM plasma, for a specific mass of DM, generally depend on the DM annihilation channels, which we assume to be a pair of electron and positron in this context. The energetic electrons transfer the energy to the photons via inverse Compton scattering, which remains effective around the epoch of recombination. At energies $\lesssim \mathcal{O}(100)$ MeV these produce photons which effectively ionize hydrogen [44–46, 48, 79, 103–105]. The electrons and photons with lower energies participate in collisional heating, excitations and ionization [44, 46, 106]. Further, the photons with higher energies can initiate an electromagnetic cascade by Compton scattering with an electron, or escape without heating the plasma [44]. Note that around the epoch of recombination ($z \simeq 1100$), the inverse Compton scattering is very efficient in transferring the energy from relativistic electrons to the photons, as the respective rate is much larger than the expansion rate of the Universe [44].

Quantitatively, the energy injection (per unit volume per unit time) from the annihilation of two DM particles, at a redshift z around the recombination epoch is given by [46, 49],

$$\frac{dE}{dV dt}(z) = \rho_{\text{crit}}^2 c^2 \Omega_c^2 (1+z)^6 P_{\text{ann}} \quad (2.1)$$

In the above equation, $P_{\text{ann}} = f_{\text{eff}}(z) \frac{\langle \sigma v \rangle}{m_\chi}$, where $\langle \sigma v \rangle$ denotes the annihilation cross-section multiplied by the relative speed of the DM particles averaged using the phase space distribution function of DM particles at redshift z , $f_{\text{eff}}(z)$ denotes the effective fraction of the injected energy absorbed by the SM plasma at redshift z ⁴, ρ_{crit} denotes the critical energy density in our Universe in the present epoch, $\Omega_{c,0}$ denotes the fractional contribution to the energy density from DM at the present epoch and c denotes the speed of light in vacuum. Around the recombination epoch ($z \simeq 1100$), which is of interest in the present context, the injected energy is distributed approximately equally contributing towards ionization and excitation of the neutral atoms, and heating the plasma. In a fully ionized plasma, the injected energy contributes to heating the plasma. Following ref. [107], an approximate estimation of the energy contributing towards ionization and excitation each fractions can be given by $(1 - x_e)/3$ while $(1 + 2x_e)/3$ contributed towards heating of the plasma, where x_e is free electron fraction. More accurate estimations for the relevant fractions have been estimated in refs. [106, 108–110]. The equation governing the evolution of the temperature of the baryons and electrons T_b is given by the Compton evolution equation,

$$(1+z) \frac{dT_b}{dz} = \frac{8\sigma_T a_R T_r^4}{3m_e c H(z)} \frac{x_e}{1 + f_{He} + x_e} (T_b - T_r) + 2T_b - \frac{2}{3k_B H(z)} \frac{\kappa_h(z)}{1 + f_{He} + x_e}, \quad (2.2)$$

where the term involving κ_h corresponds to the effect of heating from additional energy injection in the SM plasma and is given by,

$$\kappa_h(z) = \frac{(1 + 2x_e)}{3n_H(z)} \frac{dE}{dV dt}(z). \quad (2.3)$$

In the above equation, T_r denotes the radiation (photon) temperature at redshift z , σ_T denotes the Thomson scattering cross-section, a_R is the radiation constant, k_B is the Boltzmann constant, m_e is the mass of electron, c denotes the speed of light in vacuum, z denotes the redshift. Further, $H(z)$ stands for the Hubble parameter at redshift z , x_e and f_{He} denote the free electron fraction and the fraction of Helium nuclei with respect to the number of H nuclei ($n_H(z)$) present in the SM plasma at redshift z . Note that at the onset of recombination epoch Thompson scattering is effective and $T_r \simeq T_b$. During the recombination epoch, the free electrons are captured by the hydrogen (and Helium) nuclei to form neutral atoms, and around the last scattering surface, the medium becomes transparent for photons, which we observe as the CMBR. The effect of the additional energy injection on the formation of the neutral atoms, and the evolution of the free electron fraction can be described to a good approximation by the following equation [45, 46, 49]:

$$\frac{dx_e}{dz} = \frac{1}{(1+z)H(z)} [R_s(z) - I_s(z) - I_X(z)], \quad (2.4)$$

where $R_s(z)$ is the standard recombination rate, $I_s(z)$ is the ionization rate due to standard sources and $I_X(z)$ is the ionization rate due to annihilating DM particles at redshift z .

⁴The efficiency of energy injection process in the SM plasma, as a function of the redshift z , is included in the parameter f_{eff} . As demonstrated in refs. [47, 50, 103], around redshift of $z \simeq 1100$ $f_{\text{eff}}(z)$ is independent of the redshift z to a very good approximation for a particular annihilation channel. A large value of f_{eff} corresponds to instantaneous transfer of energy to the SM plasma, referred to as the ‘‘on-the-spot’’ approximation. A detailed computation of the function $f(z)$, beyond the on-the-spot approximation, can be found in ref. [50].

Considering the effective three-level-atom framework [111], to a good approximation, these are given by [45, 46, 49, 50],

$$[R_s(z) - I_s(z)] = C \left[x_e^2 n_H \alpha_B - \beta_B (1 - x_e) e^{-E_{21}/k_B T_r} \right], \quad (2.5)$$

In the above equation, n_H denotes the number density of hydrogen nuclei, α_B and β_B are the effective recombination and photoionization rates from the first excited state in Case *B* recombination, E_{21} stands for the energy difference between the $2s$ level and the ground state of Hydrogen atom and T_r is the radiation temperature. Finally, C is given by,

$$C = \frac{[1 + K \Lambda_{2s1s} n_H x_{1s}]}{[1 + K \Lambda_{2s1s} n_H x_{1s} + K \beta_B n_H x_{1s}]}. \quad (2.6)$$

where, $\Lambda_{2s1s} \simeq 8.22 \text{ s}^{-1}$ is the decay rate of the metastable $2s$ level to the $1s$ level via two photon emission, $n_H x_{1s}$ is the number density of neutral ground state H atoms, the fraction of hydrogen atoms in the $1s$ state is given by x_{1s} and $K = \frac{\lambda_\alpha^3}{8\pi H(z)}$, where $H(z)$ is the Hubble expansion rate at redshift z and λ_α is the wavelength of the Ly- α transition from the $2p$ level to the $1s$ level. Note that around the recombination epoch, as the fraction of hydrogen atoms in the $2s$ or higher states is negligible as compared to that in the $1s$ state, to a good accuracy, $x_{1s} = 1 - x_e$. As described in ref. [111], this factor C corresponds to the probability of the transition from $n = 2$ state to the ground state before getting photoionized.

Finally $I_X(z)$, which describes the effect due to annihilating DM particles, is given by $I_X(z) = I_{X_i}(z) + I_{X_\alpha}(z)$ [46, 106]. Here $I_{X_i}(z)$ denotes the contribution from direct ionization from the ground state of the hydrogen atom, thus increasing x_e with time. I_{X_α} denotes the contribution to the increment of x_e due to ionization from the $n = 2$ state. Note that the factor $(1 - C(z))$ denotes the respective ionization probability.

$$I_{X_i}(z) = -\frac{\chi_i(z)}{(1+z)H(z)n_H(z)E_i} \left(\frac{dE}{dV dt} \right),$$

$$I_{X_\alpha}(z) = -\frac{(1-C(z))\chi_\alpha(z)}{(1+z)H(z)n_H(z)E_\alpha} \left(\frac{dE}{dV dt} \right).$$

In the expressions above, $\left(\frac{dE}{dV dt} \right)$ refers to the energy injection from the annihilation of DM, as given by Eq. [2.1], $\chi_i \simeq (1 - x_e)/3 \simeq \chi_\alpha$, which denote the fractions of the injected energy which contribute towards ionization and excitation respectively. The rate of collisional excitation of hydrogen ($1s \rightarrow 2s, 2p$) due to DM annihilation is similar to that of direct ionization, and can be estimated by replacing E_i by the Lyman- α energy E_α and $\chi_i(z)$ by the fraction $\chi_\alpha(z)$ of the injected energy going into excitations. As mentioned, once an atom is in the $n = 2$ state, there is a probability $(1 - C(z))$ for it to be ionized by CMBR photons.

The enhancement of the free electron fraction around the recombination leads to broadening of the last scattering surface. Thus, the temperature and polarization power spectrum are modified. While for the TT power spectrum, the effect of annihilation generally suppresses the power at all scales, larger x_e and the increased width of the last scattering surface enhances the polarization power spectra at large scales [44]. Thus, the annihilation of DM during the recombination epoch can have a significant impact [44, 50, 53, 112, 113].

The constraints from Planck collaboration on the parameter $P_{ann} \leq 1.9 \times 10^{-7} \text{ m}^3 \text{ sec}^{-1} \text{ Kg}^{-1}$ (95% upper bound)[2], under the assumption that DM only annihilates into a pair of electron-positron [2]. Including high multipoles (l) `Plik lite` likelihood the limit is relaxed to

$P_{ann} \leq 2.34 \times 10^{-7} \text{ m}^3 \text{ sec}^{-1} \text{ Kg}^{-1}$ (95% upper bound). In this work high l TTTEEE lite, low- l TT, low- l EE, lensing data set has been used, as it reduces the computational time. However, the constraints can be relaxed by upto a factor of 2 [114]. Including Planck lensing and BAO data further tightens the constraints. For comparison, it is noteworthy that the correct relic abundance of DM via thermal freeze-out requires a thermally averaged DM annihilation cross-section in the ballpark of $\langle\sigma|v|\rangle \approx 2 \times 10^{-26} \text{ cm}^3 \text{ s}^{-1}$ [2]. Apart from affecting the recombination process, annihilation of DM in the early Universe can also affect the growth of perturbations [52]. We have checked the same for some benchmark scenarios, as mentioned in Sec. 4.1. In the present work, we have not included this effect, as it generally leads to weak constraints on the DM annihilation cross-section. Further, DM annihilation into the SM particles at lower redshift affects the reionization process [77]. We will not include such effects in the present work.

2.2 DM scattering with SM

As mentioned in the introduction, the presence of DM-electron interaction terms in the lagrangian leads to both DM annihilation into a pair of $\bar{e}e$, and DM- e scattering. In this subsection, we review the effect of DM- e scattering in the early Universe. The scattering between DM and e in the early Universe, around and before the recombination epoch, leads to the exchange of energy and momentum to the DM from the SM plasma. Thus, DM clumps less at the small scales and generally the growth of density perturbation on small length scales is suppressed. Consequently, the temperature power spectrum of the CMBR is reduced, especially in the small length scales [54, 59–61, 115].

Following refs. [54, 59, 60, 63, 64, 116], we discuss the implications of DM- e drag quantitatively in this context. The presence of DM-electron scattering leads to drag between the SM and DM fluids. Around the recombination epoch, which is of interest in the present context, both DM and baryons are non-relativistic. We denote the (non-relativistic) velocity of DM and electron by \vec{v}_χ and \vec{v}_e respectively, and the respective momenta scale as a^{-1} , where a denotes the scale factor at the same epoch. The DM particles, around the epoch of recombination ($T_r \lesssim 1 \text{ eV}$), were not in thermal equilibrium with the SM plasma, while the photons and baryons maintain the same temperature thanks to the efficient Thomson scattering, as discussed in the previous section. We denote the temperature of the baryon fluid by T_b , the respective phase space distribution function for the electrons are denoted by $f_e(v_e)$. Further, we parametrize the (unperturbed) velocity distribution function of the DM fluid $f_\chi(v_\chi)$ by an effective temperature T_χ ⁵.

In the following we review the of the DM-electron drag following ref. [63]. The drag force per unit mass of the DM, $d\vec{v}_\chi/dt$, can be obtained by estimating the momentum transfer (per unit time) to the DM particle in a scattering with an electron, and subsequently taking an average over the respective velocity distribution functions. The change in DM momentum ($\Delta\vec{p}_\chi$) per collision is, to leading order in the (non-relativistic) velocities, given by,

$$\Delta\vec{p}_\chi = \frac{m_\chi m_e}{m_\chi + m_e} |\vec{v}_\chi - \vec{v}_e| \left(\hat{n} - \frac{\vec{v}_\chi - \vec{v}_e}{|\vec{v}_\chi - \vec{v}_e|} \right) \quad (2.7)$$

where \hat{n} is the direction of the scattered DM particle in the center-of-mass frame and m_e and m_χ denote the mass of the electron and DM respectively. The acceleration experienced by

⁵For a thermal relic DM candidate, T_χ can be simply obtained from the decoupling temperature T_D , and is given by $T_\chi(z) = \frac{T_D a_D^2}{a(z)^2}$, where a_D and $a(z)$ denote the scale factors at the DM decoupling epoch and at the redshift z respectively.

the DM is then

$$\frac{d\vec{v}_\chi}{dt} = \frac{\rho_e}{m_\chi + m_e} \int dv_e v_e^2 f_e(v_e) \int \frac{d\hat{n}_e}{4\pi} \int d\hat{n} \left(\frac{d\sigma(|\vec{v}_\chi - \vec{v}_e|)}{d\hat{n}} \right) |\vec{v}_\chi - \vec{v}_e|^2 \left(\hat{n} - \frac{\vec{v}_\chi - \vec{v}_e}{|\vec{v}_\chi - \vec{v}_e|} \right) \quad (2.8)$$

where ρ_e is the energy density of the free electrons. Here $d\sigma(v)/d\hat{n}$ is the differential cross-section for electron-DM scattering in the center-of-mass frame, which is a function of the respective relative velocity $\vec{v} = \vec{v}_\chi - \vec{v}_e$ between the DM particle and electron and $\hat{n}_e = \frac{\vec{v}_e}{v_e}$. The cross-section is parametrized as a function of the relative speed v as follows,

$$\bar{\sigma}(v) = \sigma_{\text{drag}} v_r^n, \quad (2.9)$$

where n is an integer. In the present study, we will consider velocity independent drag term, i.e. $n = 0$, see e.g. [116]. Note that, in the literature generally the DM particles are assumed to have a Maxwell-Boltzmann (MB) velocity distribution, characterized by the ‘‘temperature’’ T_χ ⁶. Considering both χ and e follows MB velocity distribution, their relative velocity $\vec{v}_r = \vec{v}_\chi - \vec{v}_e$ also follows the same, with a mean relative velocity given by the difference of the respective mean velocities, and a variance $\left(\frac{T_b}{m_e} + \frac{T_\chi}{m_\chi} \right)$ per direction⁷. Further, as the present analysis involves very early Universe, the peculiar velocity has been assumed to be sufficiently small compared to the respective thermal velocities, and the dispersion in the respective relative velocities. Thus, non-linear terms involving the peculiar velocity has been neglected in estimating the drag force [56], in the case of velocity-independent drag term i.e. for $\bar{\sigma}(v) = \sigma_{\text{drag}}$. For an improved approach, see e.g. ref. [60]. A detailed discussion on the validity can be found in ref. [65].

2.2.1 Cosmological perturbations with DM - e scattering

In this subsection, we discuss the the cosmological perturbation equations governing the density and velocity perturbations of DM and baryons in the presence of DM- e interaction⁸. We adopt the synchronous gauge and follow the notations of ref. [121]. In the synchronous gauge, when DM interaction is absent, θ_χ takes a zero solution and can therefore be ignored. However, this is not possible in the presence of interactions. The density contrasts δ_χ and δ_b and divergence of (bulk) velocity θ_χ and θ_b of DM and baryons in the Fourier space,

⁶This description is accurate if the self-interaction rate of χ particles are significant (i.e. comparable or larger than the Hubble expansion rate). Also, in case of thermal relic χ particles, one may use effectively $T_\chi(z < z_D) = T_\chi(z_D) \frac{a(z_D)^2}{a(z)^2}$, where z_D denotes the redshift corresponding to thermal freeze-out of χ , and $a(z)$ denotes the scale factor at redshift z .

⁷It has been argued that, for negative n , e.g. $n = -2$ and $n = -4$, the assumption of MB distribution for DM particles χ can lead to a discrepancy in the heat exchange rate by a factor of 2-3 compared to a more accurate treatment using the Fokker-Planck approximation for the respective collision operator [117]. Note that such negative power of v can appear if DM candidate posses electric dipole moment, or for millicharged DM [115, 118–120].

⁸Although we only consider DM- e scattering, as the e , protons (and Helium ions) interact appreciably, the effect of such interaction can be treated similarly as that of DM-proton scattering [63, 116].

respectively, evolve following the differential equations [54, 57, 58, 121] :

$$\dot{\delta}_\chi = -\theta_\chi - \frac{\dot{h}}{2}, \quad \dot{\delta}_b = -\theta_b - \frac{\dot{h}}{2}, \quad (2.10)$$

$$\dot{\theta}_\chi = -\frac{\dot{a}}{a}\theta_\chi + c_\chi^2 k^2 \delta_\chi + R_\chi (\theta_b - \theta_\chi), \quad (2.11)$$

$$\dot{\theta}_b = -\frac{\dot{a}}{a}\theta_b + c_b^2 k^2 \delta_b + R_\gamma (\theta_\gamma - \theta_b) + \frac{\rho_\chi}{\rho_b} R_\chi (\theta_\chi - \theta_b). \quad (2.12)$$

In the above equations ρ_χ , ρ_b are the respective energy densities and c_χ , c_b are the speeds of sound in the DM and baryon fluids respectively given by;

$$c_\chi^2 = \frac{\dot{P}_\chi}{\dot{\rho}_\chi} = \frac{k_B T_\chi}{m_\chi} \left(1 - \frac{1}{3} \frac{d \ln T_\chi}{d \ln a} \right),$$

$$c_b^2 = \frac{\dot{P}_b}{\dot{\rho}_b} = \frac{k_B T_b}{\mu} \left(1 - \frac{1}{3} \frac{d \ln T_b}{d \ln a} \right),$$

where μ is the mean molecular weight of the baryonic fluid [121]. The overdot represents a derivative with respect to conformal time, k is the wave number of a given Fourier mode, a is the scale factor and h is the trace of the spatial part of the metric perturbation. The sound speeds c_χ , and c_b are generally different, since, the interaction of DM with the SM particles, even if non-vanishing, is assumed to be rather small. Further, $\delta_{\chi,b}$ and $\theta_{\chi,b}$ are the density fluctuations and velocity divergences respectively, of the fluids in Fourier space. In addition, the scattering between χ and e leads to heat exchange between DM and baryon fluid. This modifies the evolution of the respective temperature T_b and T_χ [63, 116],⁹

$$-(1+z)H(z)\frac{dT_b}{dz} + 2H(z)T_b = 2\frac{\mu}{m_e}R_\gamma(T_r - T_b) + 2\frac{\mu}{m_\chi}R'_\chi(T_\chi - T_b), \quad (2.13)$$

$$-(1+z)H(z)\frac{dT_\chi}{dz} + 2H(z)T_\chi = 2R'_\chi(T_b - T_\chi). \quad (2.14)$$

where T_r is the radiation (photon) temperature and μ is the mean molecular weight. The terms proportional to R_γ and R_χ in Eqs. [2.12], [2.11], [2.13] describe the momentum transfer between interacting fluids, acting as a drag force between the fluids. The momentum-transfer rate coefficient R_γ arises from Compton scattering between photons and electrons. The rate coefficient for DM-electron scattering is derived in Sec. A.2 following the ref. [60] given by,

$$R_\chi = a\rho_e \frac{\mathcal{N}_n \sigma_{\text{drag}}}{m_\chi + m_e} \left(\frac{T_\chi}{m_\chi} + \frac{T_b}{m_e} + \frac{V_{\text{rms}}^2}{3} \right)^{(n+1)/2}, \quad (2.15)$$

also,

$$R_\gamma = a \frac{4\rho_\gamma}{3\rho_b} n_e \sigma_T, \quad (2.16)$$

where σ_T is the Thomson scattering cross-section, $V_{\text{rms}}^2 = \langle \vec{V}_\chi^2 \rangle_\xi = \int \frac{dk}{k} \Delta_\xi \left(\frac{\theta_b - \theta_c}{k} \right)^2$ and $\langle \dots \rangle_\xi$ denotes an average with respect to the primordial curvature perturbation, and $\Delta_\xi \simeq 2.4 \times 10^{-9}$ is the primordial curvature variance per log k [122], σ_{drag} denotes the DM-electron scattering cross-section, $\mathcal{N}_n \equiv 2^{(5+n)/2} \Gamma(3+n/2)/(3\sqrt{\pi})$, and $\rho_e = (1 - Y_{\text{He}})\rho_b x_e m_e/m_p$ is the electron density, Y_{He} is the helium mass fraction, m_p is the proton mass and x_e is the ionization fraction. The heat-transfer rate coefficient is $R'_\chi = R_\chi m_\chi / (m_\chi + m_e)$.

⁹Similar expressions have been obtained in the context of DM-proton scattering in the literature [55, 59].

In the present context, we focus on the case where $n = 0$. In this scenario, the relative bulk velocity between the DM and baryon fluids is small compared to the thermal relative velocity between the particles, allowing us to neglect the V_{rms} term. However, for the cases where $n = -2$ and $n = -4$, the DM scattering rate is weak in the early Universe, allowing the relative bulk velocity to exceed the thermal velocity. In such cases, the V_{rms} term cannot be neglected relative to the thermal velocity, and the full expression must be used.

3 DM-electron Interaction: An Effective Operator Approach

In this section, we discuss relevant interactions of DM with e considered in the present work. In the following discussion, we assume that such interactions are mediated by very heavy mediators with the mediator mass much larger than twice the mass of DM (i.e. $2m_\chi$). Therefore, we describe the relevant interactions terms using effective operators with the following form,

$$\mathcal{L}_{\text{eff}} = g_{\text{eff}} \mathcal{O}_\chi \mathcal{O}_e. \quad (3.1)$$

In the above equation, \mathcal{O}_χ and \mathcal{O}_e are operators which are bilinear in the DM and electron fields, respectively and g_{eff} denotes the respective effective coupling. It is convenient to denote the product of these two operators as \mathcal{O}^e , where the superscript e indicates that the operator describes DM-electron interactions; $\mathcal{O}^e = \mathcal{O}_\chi \mathcal{O}_e$. More generally, several such effective operators may be present, and in such scenarios, the effective lagrangian is given by $\mathcal{L}_{\text{eff}} = \sum_i g_{\text{eff},i} \mathcal{O}_i^e$ where \mathcal{O}_i^e denotes the i^{th} operator and $g_{\text{eff},i}$ denotes the corresponding interaction strength, for details see. [123–126]. In Table. [1], we describe the lowest dimensional effective operators depicting DM- e interactions for fermionic DM (ψ), and for real scalar DM (ϕ). The respective mass dimensions of these operators are six and five for fermionic DM and real scalar DM particles respectively. Considering one type of operator at a time, we perform an expansion in the DM-electron relative speed v , and only keep the leading order term for each of these operators. The DM- e scattering cross-section for each of these operators, upto the leading order in the relative speed v between the DM particle and e or the corresponding momentum transfer \mathbf{q} , thus obtained, are mentioned in the third column. Finally, in the fourth column, the nature of (thermally) averaged DM annihilation cross-section is mentioned. Note that in this context $v_{\chi,\text{rel}}$ denotes the relative speed between the annihilating DM particles. As discussed before, the same effective operator can lead to both DM annihilation into a pair of electron and positron, and DM- e scattering. However, as the relative velocity $v_{\chi,\text{rel}}$ is non-relativistic, among the operators considered, only the ones contributing to the s -wave annihilation can be effective at late times.

In Table. [1] the operators \mathcal{O}_i^e are, thus, given by :

$$\begin{aligned} \mathcal{O}_1^e &\equiv \xi_s^\dagger \xi_s \xi_r^\dagger \xi_r, \\ \mathcal{O}_2^e &\equiv i \mathbf{s}_\psi \cdot \mathbf{q}, \\ \mathcal{O}_3^e &\equiv i \mathbf{s}_e \cdot \mathbf{q}, \\ \mathcal{O}_4^e &\equiv (\mathbf{s}_\psi \cdot \mathbf{q})(\mathbf{s}_e \cdot \mathbf{q}), \\ \mathcal{O}_5^e &\equiv \mathbf{s}_\psi \cdot \mathbf{v}_e^\perp, \\ \mathcal{O}_6^e &\equiv i \mathbf{s}_\psi \cdot (\mathbf{s}_e \times \mathbf{q}), \\ \mathcal{O}_7^e &\equiv \mathbf{s}_e \cdot \mathbf{v}_e^\perp, \\ \mathcal{O}_8^e &\equiv \mathbf{s}_\psi \cdot \mathbf{s}_e. \\ \mathcal{O}_9^e &\equiv i \mathbf{s}_e \cdot (\mathbf{q} \times \mathbf{v}_e^\perp), \end{aligned}$$

S.No	Operator (\mathcal{O}_i^e)	$\mathcal{M}_{\text{drag}} \propto$	$\langle \sigma v_{\chi, \text{rel}} \rangle$ (s-wave ?)
F_1	$\bar{\psi}\psi\bar{e}e$	$4m_\psi m_e \mathcal{O}_1^e$	No
F_2	$\psi\gamma^5\bar{\psi}\bar{e}e$	$4m_e \mathcal{O}_2^e$	Yes
F_3	$\psi\psi\bar{e}\bar{\gamma}^5 e$	$-4m_\psi \mathcal{O}_3^e$	No
F_4	$\psi\gamma^5\bar{\psi}\bar{e}\bar{\gamma}^5 e$	$-4\mathcal{O}_4^e$	Yes
F_5	$\psi\gamma^\mu\bar{\psi}\bar{e}\bar{\gamma}_\mu e$ (vanishes for Majorana ψ)	$4m_\psi m_e \mathcal{O}_1^e$	Yes
F_6	$\psi\gamma^\mu\bar{\psi}\bar{\gamma}^5\bar{e}\bar{\gamma}_\mu e$	$8m_\psi m_e (\mathcal{O}_5^e - m_e \mathcal{O}_6^e)$	No
F_7	$\psi\gamma^\mu\bar{\psi}\bar{e}\bar{\gamma}_\mu\bar{\gamma}^5 e$ (vanishes for Majorana ψ)	$-8m_e (m_\psi \mathcal{O}_7^e + \mathcal{O}_6^e)$	Yes
F_8	$\psi\gamma^\mu\bar{\psi}\bar{\gamma}^5\bar{e}\bar{\gamma}_\mu\bar{\gamma}^5 e$	$-16m_\psi m_e \mathcal{O}_8^e$	$\propto m_e^2/m_\psi^2$
F_9	$\bar{\psi}\sigma^{\mu\nu}\psi\bar{e}\sigma_{\mu\nu}e$ (vanishes for Majorana ψ)	$32m_e m_\psi \mathcal{O}_8^e$	Yes
S_1	$\mathcal{O}_{e\phi}^S = (\phi^\dagger\phi)(\bar{e}e)$	$2m_e \mathbb{I}_e$	Yes
S_2	$\mathcal{O}_{e\phi}^P = (\phi^\dagger\phi)(\bar{e}\bar{\gamma}^5 e)$	$2m_e \mathcal{O}_9^e$	Yes

Table 1: Summary of effective operators and the respective DM- e scattering cross-section σ_{drag} . In the right column, s-wave indicates whether the DM annihilation cross-section is s-wave dominated [124–126].

In the above expressions, $\mathbf{s}_\psi = \xi_s^\dagger \vec{\sigma} \xi_s$, $\mathbf{s}_e = \xi_r^\dagger \vec{\sigma} \xi_r$ and \mathbf{q} denotes the momentum transfer as described above, $\mathbf{v}_e^\perp = \frac{\mathbf{p}_1 + \mathbf{p}_2}{2m_\psi} - \frac{\mathbf{k}_1 + \mathbf{k}_2}{2m_e}$. In the subsequent sections, we describe the implications of DM annihilation and scattering with electrons in the light of CMBR data.

4 Results

The effect of DM annihilation and scattering with electrons in the very early Universe, around the epoch of recombination, can be captured by two parameters, P_{ann} and σ_{drag} respectively. As the presence of DM-electron interaction terms in the lagrangian leads to both DM annihilation into a pair of electron and positron, and scattering between DM and electron, we extend the six parameters of the base Λ CDM by these two additional parameters σ_{drag} and P_{ann} . The base parameters are: ω_b (baryon density), ω_c (dark matter density), θ_s (sound horizon angle), A_s (scalar perturbation amplitude), n_s (spectral index), and τ_{reio} (reionization optical depth).

We have used a modified version [59] of CLASS [100, 101] to solve the relevant equations Eq. [2.11] and Eq. [2.12] to estimate the TT, EE power spectrum. The likelihood for the model parameters is estimated using the Bayesian statistics with suitable priors. Using Markov Chain Monte Carlo (MCMC) method, with the help of MontePython [102], then, the maximum likelihood and the confidence intervals are determined. In particular, we obtain the 95% upper limit on the parameters P_{ann} and σ_{drag} . These upper limits are then used to obtain constraints on the interaction strengths of the effective operators, as mentioned in Table. [2].¹⁰

¹⁰The obtained chains are tested using the Gelman-Rubin criterion (R-1 convergence criterion). The commonly used threshold is $R-1 < 0.02$. However, for the `lite` dataset in the case of annihilation, we observed

Note that, in the present study, the terms involving DM annihilation in the relevant perturbation equations have not been considered. We have checked that it does not affect the constraints appreciably. Further, we have not included the contribution of the drag term in the temperature evolution, as described in Eq. [2.13] for the same reason.

4.1 Likelihood analysis and Constraints of Cosmological Parameters

In this section, we describe the constraints on the parameters (P_{ann} and σ_{drag}) relevant for describing the DM interactions, in the light of CMBR data. For the analysis, we have used the Planck 2018 baseline data set, which includes high- ℓ TT+TE+EE, low- ℓ TT, low- ℓ EE and Planck lensing data.

As mentioned above, we have used a modified version of the publicly available code [59] CLASS [100, 101] together with the MCMC simulator MontePython [102] to obtain the posterior distributions of the parameters considered in our study. We have varied the mass of DM as follows : $m_\chi \in \{1 \text{ MeV}, 10 \text{ MeV}, 100 \text{ MeV}, 1 \text{ GeV}, 10 \text{ GeV}\}$. Further, assuming flat priors, the following upper limits on the flat priors for the relevant cosmological parameters, respectively for the DM masses we considered:

$$\sigma_{\text{drag}} = [1 \times 10^{-24}, 2 \times 10^{-24}, 3 \times 10^{-22}, 3 \times 10^{-21}, 3 \times 10^{-20}], \quad (4.1)$$

$$P_{\text{ann}} = [3 \times 10^{-6}, 2 \times 10^{-6}, 4 \times 10^{-6}, 3 \times 10^{-6}, 3 \times 10^{-6}]. \quad (4.2)$$

The respective lower limits are set to 0.

DM mass (m_χ)	σ_{drag} (95% C.L)	P_{ann} (95% C.L)	σ_{drag} ($P_{\text{ann}} = 0$)(95% C.L)
1 MeV	1.38×10^{-26}	2.31×10^{-7}	1.22×10^{-26}
10 MeV	9.75×10^{-26}	2.34×10^{-7}	8.70×10^{-26}
100 MeV	9.43×10^{-25}	2.38×10^{-7}	8.3×10^{-25}
1 GeV	9.44×10^{-24}	2.406×10^{-7}	8.5×10^{-24}
10 GeV	10.3×10^{-23}	2.41×10^{-7}	9.44×10^{-23}

Table 2: Constraints on σ_{drag} (in cm^2) and P_{ann} (in $\text{m}^3/\text{sec}/\text{kg}$) for different m_χ .

In Table. [3], the results of the statistical analysis have been mentioned for $m_\chi = 1 \text{ MeV}$. In particular, the best fit values and the limits on the relevant parameters (Ω_b , Ω_{drag} , θ_s , A_s , n_s and τ_{reio}) (at 1σ and at 2σ) have been shown. For different m_χ , as described above, the results of the statistical analysis are presented in Table. [2]. In particular, in this table, the limits (at 95% C.L.) on $\sigma_{\text{drag}}(\text{cm}^2)$ and $P_{\text{ann}}(\text{cm}^3/\text{sec}/\text{kg})$ are mentioned for the different choices of m_χ . In right panel of Fig. [1], the 95% upper limits on the parameter P_{ann} for different masses of DM (m_χ) have been shown. The solid line depicts the annihilation parameter P_{ann} in the absence of the drag term, obtained using the same dataset, as mentioned above. Note that, in the absence of the drag term, the upper limit on P_{ann} is independent of the mass of DM m_χ . However, as shown in the right panel of Fig. [1], when DM annihilation into $\bar{e}e$, as well as DM-electron scattering effects are considered, the constraints on the parameter P_{ann} shows moderate dependence of m_χ . The variation is less than $\mathcal{O}(10)\%$, considering m_χ within the range 1 MeV to 10 GeV. This can be inferred from Eq. [2.11] and Eq. [2.16], as for a fixed P_{ann} and σ_{drag} , the parameter R_χ varies with m_χ . Consequently, the best fit and

a change in the 95% C.L. value even below this threshold. Therefore, we used a stringent criterion to ensure convergence, $R-1 < 0.002$.

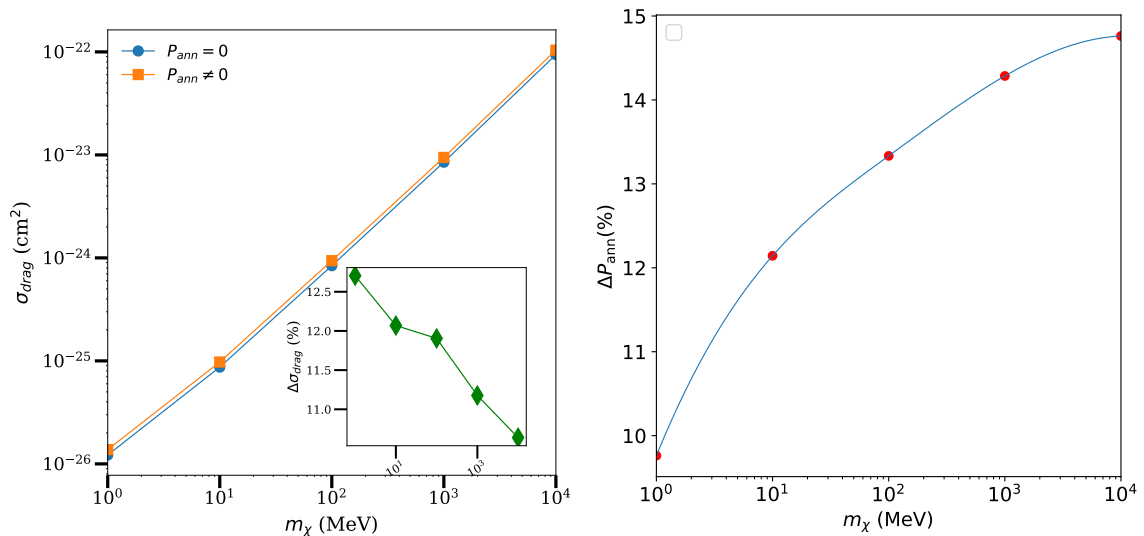


Figure 1: In the left panel, the 95% upper bound on σ_{drag} is presented for various dark matter masses with $P_{\text{ann}} = 0$, along with the corresponding upper bound on σ_{drag} when both annihilation and drag effects are considered. The bottom right panel illustrates the percentage difference between these two values. In the right panel, 95% upper bound of P_{ann} for different m_χ . The solid green line demonstrates the 95% upper limit on the parameter P_{ann} , obtained using the same dataset, in the absence of DM-electron scattering.

the 95% upper limits on P_{ann} (and σ_{drag}) are dependent on m_χ . Further, this figure shows that the constraints on P_{ann} are relaxed by approximately 10-15% in the presence of σ_{drag} as compared to the case when only P_{ann} is considered, i.e. σ_{drag} is set to 0.

In the left panel of Fig. [1], 95% C.L. upper limits on σ_{drag} have been shown for various m_χ . For smaller m_χ , the number density of the DM is large, and the probability of the scattering events are higher. The effect of DM-electron scattering, for a given cross-section σ_{drag} , would be more prominent for lighter DM. This can lead to an increase in the DM flux incident on an electron and thus, enhance the number of DM-electron scattering events.¹¹ Consequently, as shown in the left panel of Fig. [1], the upper limits on σ_{drag} is relaxed with as the mass of DM is increased. Also, the same figure shows that the bound on the scattering cross-section (σ_{drag}) is relaxed for the entire range of m_χ , in the presence of DM annihilation. The percentage change, given by $\Delta\sigma_{\text{drag}}\% = \frac{\sigma_{\text{drag}}(P_{\text{ann}} \neq 0) - \sigma_{\text{drag}}(P_{\text{ann}} = 0)}{\sigma_{\text{drag}}(P_{\text{ann}} = 0)} \times 100$, is about 10%.

In order to further understand the effect of the DM interactions on the CMBR anisotropy, in Fig. [2] we present the percentage deviation in the power spectrum of the temperature anisotropy (C_l^{TT}) and E-mode polarization anisotropy (C_l^{EE}) as a function of the multipole moment l due to DM interactions for $m_\chi = 100$ MeV. In the left panel, $\Delta C_l^{TT} = \frac{C_{lc}^{TT} - C_l^{TT}}{C_l^{TT}} \times 100$ has been shown, where C_{lc}^{TT} and C_l^{TT} denote the respective power of the two point correlations of temperature anisotropy at multipole l with and without DM inter-

¹¹In addition, the relative (thermal) speed of light DM particles, for a fixed T_χ , would be higher. Although, around the epoch of recombination, T_b is generally significantly larger than T_χ , and thus, the thermal velocity of the electrons are dominant.

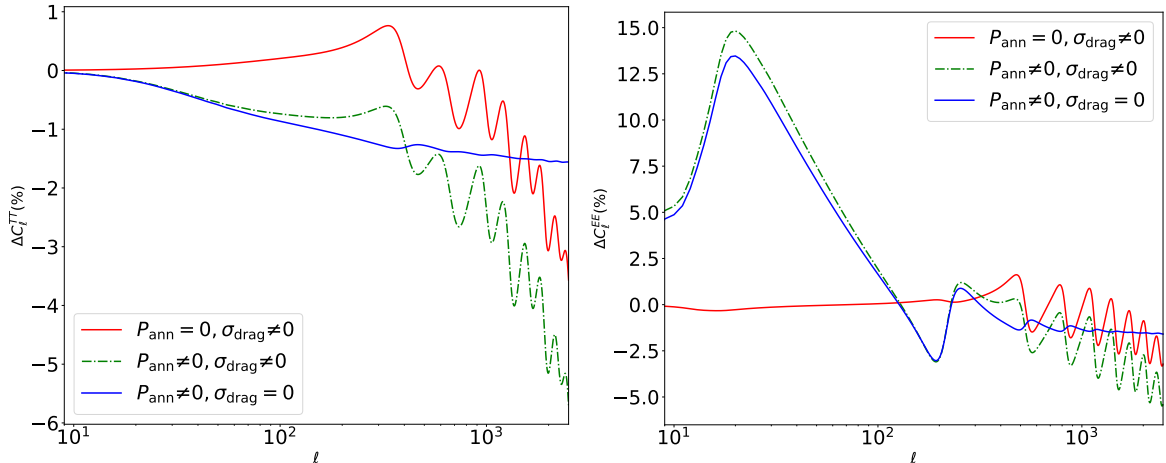


Figure 2: Comparison of the effect of DM-Electron scattering with annihilation on the TT power spectrum for DM mass $m_\chi = 100$ MeV. For each curve, we fixed $\sigma_{\text{drag}} = 9.44 \times 10^{-25}$ cm² and $P_{\text{ann}} = 2.38$ m³/s/kg to its corresponding 95% C.L. value obtained with CMBR data.

actions respectively. Similarly, the left panel shows $\Delta C_l^{EE} = \frac{C_{lc}^{EE} - C_l^{EE}}{C_l^{EE}} \times 100$, where C_{lc}^{EE} and C_l^{EE} denote the respective power of the two point correlations of E-mode polarization anisotropy at multipole l with and without DM interactions respectively. In this figure, the best-fit values for the cosmological parameters in the Λ CDM have been used, and for the additional parameters σ_{drag} and P_{ann} , the 95% upper limit, as described in Table. [2] have been used.

Note that, the presence of the drag term with electrons contributes to the increase of the rate of change of θ_χ and thus, adversely affects the growth of density contrast of DM, δ_χ . This effect is particularly prominent in the smaller length scales, (thanks to a sizable c_χ) i.e. for larger multipole moments l . This leads to a depletion in the temperature power spectrum for higher multipole moments l , as shown in the left panel of Fig. [2]. A similar trend is observed for the polarization power spectrum for larger multipole moments, as demonstrated in the right panel of the same figure. Further, in the presence of DM-electron scattering term DM is dragged by baryons, as baryons undergo oscillations around the recombination epoch. This affects the baryon loading, enhancing the power spectrum in the large length scales, (i.e. k is sufficiently small) [59, 127, 128], which leads to the rise in the temperature correlation ΔC_l^{TT} . As demonstrated in the left panel of Fig. [2], the temperature power spectrum is enhanced for smaller multipoles ($l \lesssim 320$).

As discussed in previously, the effect of DM annihilation into $\bar{e}e$ raises the baryon temperature T_b (as compared to the scenario, where such annihilation is absent) in addition to increasing the free electron fraction x_e around the last scattering surface. The consequent increase in the optical depth, in turn, depletes the temperature power spectrum at all length scales. Thus, both drag and annihilation affects the CMBR anisotropy in similar way, especially for large multipole moments l . In the left panel and in the right panel of Fig. [2], these effects are demonstrated. However, in presence of DM annihilation into $\bar{e}e$, as the free electron fraction x_e is enhanced, the polarization (E mode) power spectrum shows substantial increase for large length scales ($2 \lesssim l \lesssim 200$), as demonstrated in Fig. [2].

From the above discussion, it is evident that, although in the small length scales the effects of drag and annihilation can lead to depletion of power, their effects can be very different in the larger length scales. Consequently, negligible correlation is observed the respective posterior distributions, which is shown in Fig. [4] for $m_\chi = 10$ MeV.

As discussed, for heavier m_χ , the number of the scattering events decrease for the same cross-section σ_{drag} . Consequently, the upper limit on the scattering cross-section σ_{drag} is enhanced to achieve similar fit to the CMBR anisotropy data, which is demonstrated in the left panel of Fig. [1]. The depletion of the temperature power spectrum at large k is generally slightly reduced (for the 95% C.L. upper limit on σ_{drag} for larger m_χ . In the small k region, similar to the case of a lighter DM, a small rise in the temperature power is observed. The 95% upper limit on P_{ann} is somewhat relaxed. We find that the upper limit on P_{ann} is in agreement with the limit obtained without considering the drag term with electrons to about $\lesssim 10\%$, as shown in the same figure. A depletion of power in the small scales can also be seen from the matter power spectrum, as shown in Fig. [3], when DM-electron drag term is considered. The corresponding large k modes enter the horizon earlier in the radiation dominated Universe.

Note that using Planck data (Planck TT, TE, EE+lowE+lensing), the constraints on the DM annihilation parameter P_{ann} , for s-wave annihilation, is given by $2.33 \times 10^{-28} \text{ cm}^3 \text{ s}^{-1} \text{ GeV}^{-1}$ or equivalently, $1.9 \times 10^{-7} \text{ m}^3 \text{ s}^{-1} \text{ kg}^{-1}$ at 95% confidence level [2].¹² The upper limit on this parameter is independent of the mass of annihilating DM m_χ , and is also independent of specific annihilation channels for annihilation into the standard model particles (except neutrinos). On the averaged annihilation cross-section $\langle\sigma v\rangle$, for a fixed m_χ , the strongest constraints are obtained for DM annihilation into $\bar{e}e$. This is because, in this scenario, the injected energy thermalizes with the SM plasma almost instantly, and consequently, the fraction of the energy absorbed remains large and is independent of the redshift around the epoch of recombination (i.e., $f_{\text{eff}}(z) \simeq f_{\text{eff}}$) [2, 47, 50]. We obtain the value of f_{eff} for different DM masses from refs. [2, 47, 50]. The constraint on P_{ann} has profound implications for the thermal production of DM particles in the early Universe, particularly via s-wave annihilation into SM particles. The corresponding lower bounds on m_χ range from $m_\chi \geq 9$ GeV for annihilation into $\tau^+\tau^-$ pairs, up to $m_\chi \geq 30$ GeV for annihilation into $\bar{e}e$ pairs. Assuming thermal DM production, the 95% confidence level (CL) lower bound on the DM mass is $m_\chi \geq 40$ GeV¹³ for annihilation into $\bar{e}e$ pairs using the `lite` dataset. When both scattering and annihilation processes are considered together, the constraint on the annihilation cross-section is relaxed, lowering the bound on the DM mass for thermally produced DM in the early Universe to $m_\chi \geq 32$ GeV. This trend is expected to hold for the full Planck dataset, though the numerical values could change by a few percent.

The correlations of various cosmological parameters, in Fig. [4], the 1- σ and 2- σ posterior contours have been shown for $m_\chi = 100$ MeV. For different values of m_χ we considered, the nature of these contours and correlations among different parameters demonstrate a similar trend. We particularly focus on the correlations with various cosmological parameters with the parameters in the DM sector, i.e. $\omega_c(\Omega_c = \omega_c h^2)$, P_{ann} and σ_{drag} .

Fig. [4] demonstrates that σ_{drag} and P_{ann} are constrained by the CMBR data. The

¹²As mentioned, in this work, we have used the `Planck lite` data set in our analysis. We have checked that the upper limit on P_{ann} , as obtained with $\sigma_{\text{drag}} = 0$, differs if the full Planck data set is used instead.

¹³For the full Planck dataset, which attempted to constrain P_{ann} without invoking the drag term, the s-wave annihilation cross-section into the $\bar{e}e$ channel, required to satisfy the correct thermal relic abundance, is disfavored for $m_\chi \leq 30$ GeV [2].

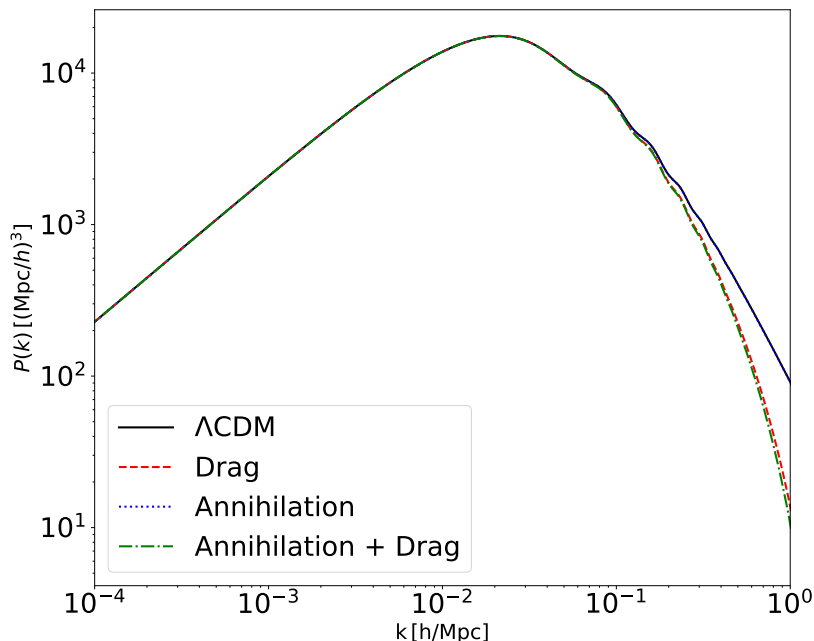


Figure 3: The effect of DM-electron scattering with annihilation on the matter power spectrum for DM mass $m_\chi = 100$ MeV. For each curve, we fixed $\sigma_{\text{drag}} = 9.44 \times 10^{-25} \text{ cm}^2$ and $P_{\text{ann}} = 2.38 \text{ m}^3/\text{s}/\text{kg}$ to its corresponding 95% C.L. value obtained with CMBR data.. The lines for Annihilation and ΛCDM overlap at high k (small length scales), with differences appearing only at very low k (large length scales), where there is a small bulge around 10^{-5} .

respective best-fit values are smaller than the upper limit by an order of magnitude. Further, the contours terminate at the lower limit on the prior (i.e. 0). Thus, setting σ_{drag} and P_{ann} to 0 (i.e. the base ΛCDM) is consistent with the data. Note that, no correlation between these two parameters is observed. However, for σ_{drag} , we observe noticeable positive correlation with n_s . This may be understood from the fact that a larger σ_{drag} prohibits the growth of the DM density contrast, especially at small length scales. In the left panel of Fig. [2], the suppression in the TT spectrum at small length scales (corresponding to the higher multipole moments), in the presence of the drag term, have been shown. This may be partly compensated by raising the scalar spectral index n_s , which enhances the primordial scalar power at these scales. There is a small positive correlation observed between ω_{drag} and σ_{drag} . This may be understood as follows: increasing σ_{drag} leads to depletion in the growth of the DM density contrast. This may be partly compensated by also increasing the DM abundance, thus enhancing ω_c . Further, similar to the ΛCDM model, (with only gravitationally interacting DM) sizable negative correlation between the Hubble parameter at the present epoch H_0 and ω_c is also observed. This is understood as increasing ω_c enhances the distance to the first peak. Consequently, as the angle θ_s is tightly constrained by the observation, H_0 is decreased. There is no noticeable (negative) correlation between n_s and P_{ann} . Note that the polarization data can remove any degeneracy in this case [44]. Finally, a strong negative correlation is observed between the parameters σ_8 (which depicts the matter power at 8 Mpc), and σ_{drag} . In the following subsection, in the context of σ_8 tension, we discuss this in some detail.

In general, it is possible that multiple operators contribute to DM annihilation and drag interactions, and different operator may dominate each of these processes. For example, the

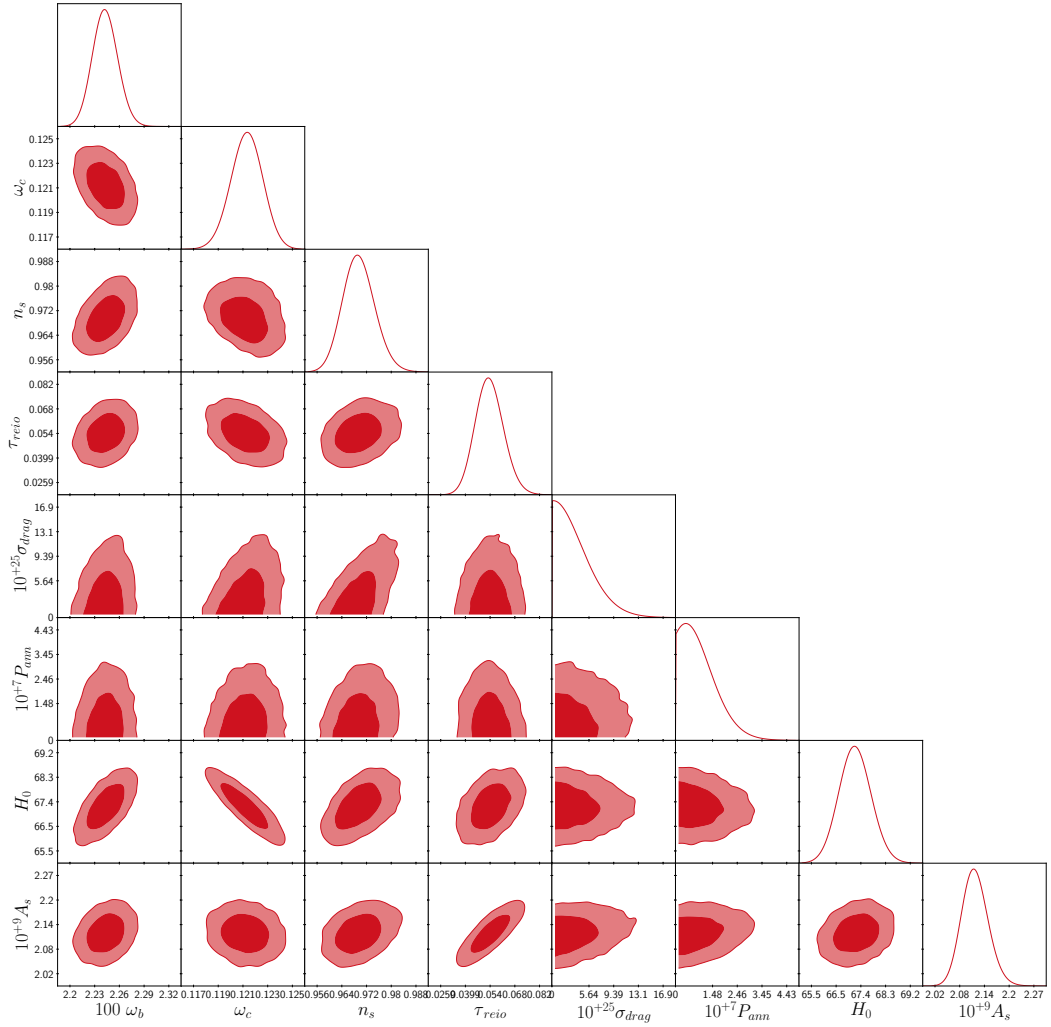


Figure 4: 1-d posterior distribution of 6+2 parameter model with parameters ω_b , ω_{drag} , θ_s , A_s , n_s , τ_{reio} , σ_{drag} , P_{ann} for $m_\chi = 100$ MeV.

Param	best-fit	mean $\pm\sigma$	95% lower	95% upper
$100 \omega_b$	2.238	$2.241^{+0.016}_{-0.015}$	2.211	2.272
ω_c	0.1209	$0.121^{+0.0013}_{-0.0014}$	0.1184	0.1237
n_s	0.9656	$0.9695^{+0.0046}_{-0.0054}$	0.9595	0.9798
τ_{reio}	0.05328	$0.05411^{+0.0074}_{-0.0077}$	0.0387	0.06949
$10^{+25} \sigma_{\text{drag}}$	0.6452	$3.667^{+0.91}_{-3.7}$	–	9.449
$10^{+7} P_{\text{ann}}$	0.4515	$0.9729^{+0.25}_{-0.97}$	–	2.38
H_0	67.08	$67.19^{+0.56}_{-0.56}$	66.07	68.29
$10^{+9} A_s$	2.106	$2.121^{+0.032}_{-0.034}$	2.054	2.185

Table 3: Statistical result of 6+2 parameter model with parameters ω_b , ω_{cdm} , H_0 , A_s , n_s , τ_{reio} , σ_{drag} , P_{ann} for $m_\chi = 100$ MeV.

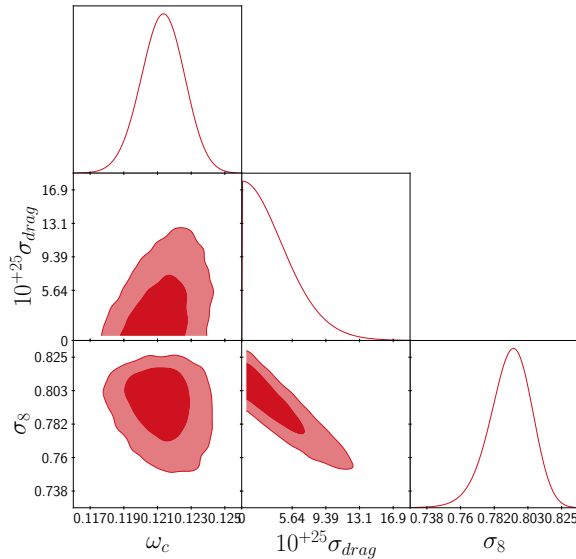


Figure 5: Posterior distribution among ω_c , σ_{drag} and σ_8 for $m_\chi = 100$ MeV.

operator F_1 can contribute significantly to the drag effect, while F_2 , as given in Table. [1], can contribute dominantly to the annihilation process.¹⁴ In the present context, we take an agnostic approach and treat these processes independently.

As mentioned, our primary focus is on a velocity-independent drag cross-section, corresponding to $n = 0$ in Eq. [2.16]. The effect of DM-electron (and also DM-proton) scattering with velocity-dependent scattering cross-sections (i.e., $\bar{\sigma}(v_r) = \sigma_{\text{drag}} v_r^n$ for $(n = -2, n = -4)$, in the absence of DM annihilation (i.e. with $P_{\text{ann}} = 0$), have been previously studied in refs. [60, 118–120, 129, 130] In the following, we briefly discuss such a possibility in the presence of s -wave annihilation of DM into $e\bar{e}$. For instance, in the case of $n = -4$, the upper limit on P_{ann} at the 95% C.L. is $2.3 \times 10^{-7} \text{ m}^3 \text{ s}^{-1}$ for a DM mass of 1 MeV and $2.2 \times 10^{-7} \text{ m}^3 \text{ s}^{-1}$ for 1 GeV. Thus, we find that the constraints on P_{ann} vary with m_χ in this scenario. Further, the upper limits on DM-electron drag parameter (σ_{drag}), in the presence of DM annihilation, are generally relaxed by $\mathcal{O}(10)\%$, depending on the choice of m_χ . For $n = -2$ and $n = -4$, the DM an improved treatment of the peculiar velocity has been followed, as it may not generally be small compared to the thermal velocity dispersion during the relevant epochs [55, 57].

4.1.1 Comment on S_8 or σ_8 Tension

The S_8 parameter is defined as

$$S_8 \equiv \sigma_8 \left(\frac{\Omega_m^0}{0.3} \right)^{0.5}, \quad (4.3)$$

where $\Omega_m^0 \equiv \rho_m^0 / \rho_{cr}^0$ is the density of matter today as a fraction of the critical density ρ_{cr}^0 , and σ_8 measures the rms amplitude of linear matter density fluctuations over a sphere of radius $R = 8 \text{ Mpc}/h$ at $z = 0$:

$$\sigma_8^2 = \frac{1}{2\pi^2} \int \frac{dk}{k} W^2(kR) k^3 P(k), \quad (4.4)$$

¹⁴Further, it may be possible that DM annihilates into $e\bar{e}$, while the drag with the SM plasma is dominated by DM-proton interactions, especially for $m_\chi \lesssim m_p$, where m_p denotes the mass of the proton.

where $P(k)$ is the linear matter power spectrum today and $W(kR)$ is a spherical top-hat filter of radius $R = 8 \text{ Mpc}/h$.

Param	best-fit	mean $\pm\sigma$	95% lower	95% upper
$10^{+25}\sigma_{\text{drag}}$	0.6452	$3.667^{+0.91}_{-3.7}$	–	9.445
σ_8	0.8102	$0.7942^{+0.02}_{-0.011}$	0.7611	0.8209

Table 4: Results for σ_8 with σ_{drag} for DM of mass 100 MeV.

There is a slight tension emerging between S_8 (or σ_8) as measured from late-Universe datasets [94, 131] and as indirectly inferred by the CMBR [1, 2], i.e., by constraining the Λ CDM parameters from the CMBR and calculating the resulting S_8 (or σ_8). In particular, weak lensing surveys such as Kilo Degree Survey (KiDS) measure $S_8 = 0.759 \pm 0.024$ [94, 95, 132], and clustering surveys like Baryon Oscillation Spectroscopic Survey (BOSS) also consistently find low S_8 (or σ_8) [96–98, 133]. Dark Energy Survey (DES) measures $S_8 = 0.776 \pm 0.017$ ($\sigma_8 = 0.733 \pm 0.0060$) [99, 131] (a combined analysis of the clustering of foreground galaxies and lensing of background galaxies). These numbers should be compared to the indirect CMBR constraint of $S_8 = 0.834 \pm 0.016$ ($\sigma_8 = 0.811 \pm 0.0060$) from Planck and ground based Experiment eg. Atacama Cosmology Telescope (ACT) and South Pole Telescope (SPT)[134–136].

In the presence of DM-e interaction, we observe a negative correlation between the parameter σ_8 and the scattering parameter σ_{drag} . This result is consistent with ref. [] where DM-proton drag was considered. A non-vanishing σ_{drag} leads to a lower value of σ_8 compared to the standard Λ CDM model, potentially alleviating the σ_8 tension. This suggests that interactions in the dark sector can play a role in resolution of the tension. However, a more detailed investigation using late-time datasets (such as KiDS), is necessary for a robust conclusion.

4.2 Constraints on lagrangian Parameters

In this section, we describe the implications of the constraints on σ_{drag} and P_{ann} for the lagrangian parameters describing the effective DM-electron interactions. Note that, when DM annihilation into $e\bar{e}$ is kinematically viable, the upper limits on both σ_{drag} and P_{ann} can lead to constraints on g_{eff} . However, generally, more than one effective operator can be present, and different operators may contribute to the (velocity-independent) annihilation and drag. Further, the annihilation and drag with two different species may be present. We find that the constraints on an effective interaction strength g_{eff} , as derived from the upper limit on P_{ann} is generally stronger as compared to the constraint on the same parameter derived from σ_{drag} . Consequently, the upper limits on P_{ann} for velocity-independent annihilation processes, as obtained in the presence of a drag term (i.e. keeping both P_{ann} and σ_{ann} as independent parameters) have been used to constrain the respective lagrangian parameters describing DM-e interactions.

The upper limits on P_{ann} have been presented in Table. [2]. The relevant expressions for scattering and annihilation cross-sections, which depend on the respective lagrangian parameters g_{eff} and m_χ , are given in Appendix. A. As mentioned, we are interested in velocity-independent operators (i.e operator F_5, F_8, F_9, S_1, S_2 given in the Table. [1]). Considering one such operator at a time, the constraints on the respective couplings have been shown in Fig. [6]. We observe that the upper limits on the vector operator (F_5) and tensor operator

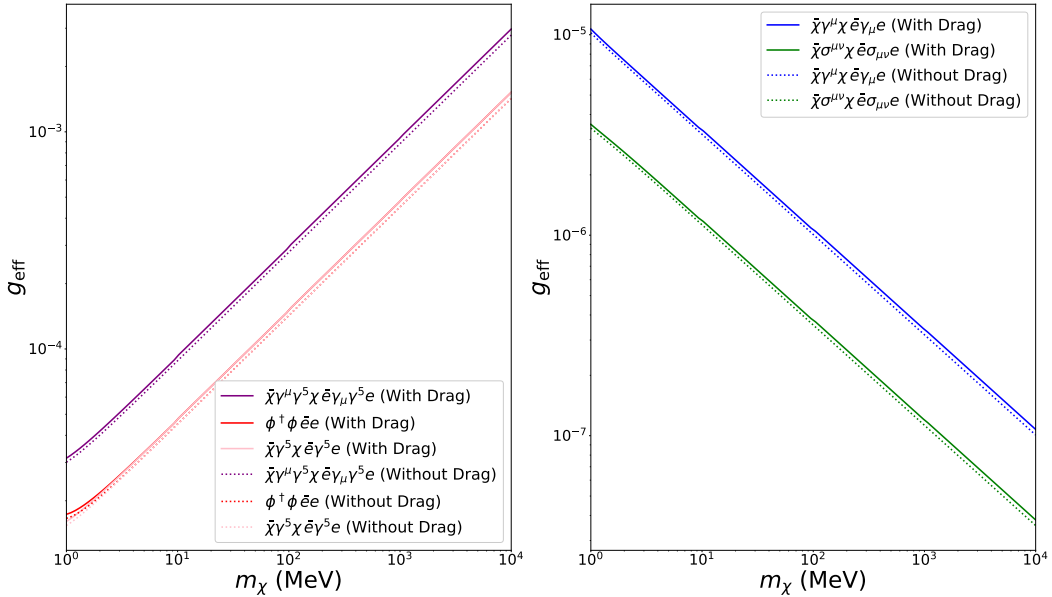


Figure 6: Constraints on the g_{eff} vs. m_χ plane from DM- e DM annihilation. g_{eff} is in unit of $[(\text{GeV})^{-2}]$ for fermionic dark matter and $[(\text{GeV})^{-1}]$ for scalar dark matter. The solid and dashed blue, purple, green and red lines correspond to bounds from annihilation (with or without drag) respectively, for vector (F_5), Pseudo-vector (F_8), Tensor (F_9), Scalar dark matter (S_1) operator as given in Table. [1] of DM- e interaction. The constraints when only drag is considered are studied in previous studies [63], however the most stringent bound arises from the annihilation of DM into e .

(F_9) decrease with m_χ , while the pseudo-vector operator (F_8) and scalar DM operator (S_1) increase with m_χ . This behavior can be explained as follows. For $m_\chi \gtrsim 1$ GeV, the effective coupling is proportional to $1/m_\chi$ for the vector (F_5) and tensor (F_9) operators, whereas for the pseudo-vector (F_8) and scalar dark matter (S_1) operators, it is proportional m_χ , the detailed expressions have been provided in Appendix B.

In the following, we compare the constraints on the effective interaction strengths, as shown in Fig. 6 with similar constraints from direct detection experiments [35, 137–142]. Among the direct detection bounds, the leading constraints from SENSEI and DAMIC-M [34, 143, 144] cover the range from 500 keV to 20 MeV. In the range of 20 MeV to 60 MeV, the strongest bounds come from the PANDAX-II [141] experiment, while for DM masses above 30 MeV up to the GeV scale, the leading constraints are provided by the XENON-1T [140] experiment. The constraint on g_{eff} from direct detection experiments for the mass range 1 MeV – 100 MeV is between $\mathcal{O}(1)$ and $\mathcal{O}(10^{-4})$, respectively, for all given operators. In this mass range, the strongest constraints for all operators come from CMB. Further, the constraints from PLANCK are more stringent as compared to the same obtained from indirect searches in the [23].

5 Conclusions

In this work, the effect of DM-electron interaction has been considered in the light of CMBR data. It has been assumed that such interactions, at the level of lagrangian, can be described

by effective operators. This description holds good when the mediators of such interactions are very heavy as compared to the energy scale of the relevant scattering or annihilation processes. The presence of DM-electron interaction terms lead to annihilation of a pair of DM into a pair of $\bar{e}e$, as well as, scattering of DM particles with free electrons present around the epoch of recombination. These processes may be governed by one or more effective operators, which may be present in the interaction lagrangian.

Around the recombination epoch, the annihilation of DM can inject energy in the plasma which can enhance the ionization of the neutral hydrogen atoms, affecting the optical depth around the recombination epoch. Further, such annihilation processes increase the free electron fraction, which can affect the polarization of the CMBR photons. DM-electron scattering leads to a non-vanishing drag between these two species. This depletes the matter power at rather small length scales. The effect can be opposite at rather larger length scales, which is possibly due to an enhanced contribution to the baryon loading, as DM is dragged by baryons. The effects of DM annihilation and drag have been separately considered in the literature, as we discussed. In this analysis, it has been emphasised that, as both of these processes stem from the same effective lagrangian terms, therefore, generally, both annihilation and scattering need to be considered while considering interacting DM scenario. Note that, for $m_\chi \gtrsim 0.51$ MeV, DM annihilation into $\bar{e}-e$ is kinematically viable. Thus, an extension of the standard model of cosmology Λ CDM has been studied including two additional parameters P_{ann} and σ_{drag} representing the effects of DM annihilation and drag with electrons, respectively. Only s -wave annihilation and velocity-independent drag has been considered in the present study. Further, following the literature, DM particles are assumed to have an effective temperature T_χ around the epoch of recombination. As DM is very weakly coupled to the SM plasma, the respective sound speeds have been assumed to be independent. Note that kinetic equilibrium in the DM sector at a temperature T_χ , generally requires sizable DM-DM interactions around the same epoch. While such an interaction may be achieved with very light mediators in the DM sector, such additional interactions have not been considered in the present context. We plan to address it in a future study.

We used (a modified version of) the publicly available code `CLASS` and MCMC code `MontePython` to estimate the posterior distribution of the relevant parameters using the `Planck-2018` data set (high l TTTEEE lite, low- l TT, low- l EE, lensing) dataset for the present analysis. We find that the presence of both annihilation and drag affects the (95% c.l.) upper limits on the respective parameters P_{ann} and σ_{drag} . It has been observed that the upper limits on σ_{drag} is relaxed by $\mathcal{O}(10)\%$, as compared to the scenario with P_{ann} is set to zero. The constraints on P_{ann} shows moderate dependence on mass of DM, especially for light DM with mass of $\mathcal{O}(1)$ MeV - $\mathcal{O}(10)$ GeV, which we considered. A relaxed upper limit on P_{ann} can somewhat reduce the lower limit on m_χ to be a viable thermal DM, assuming that s -wave DM annihilation into $\bar{e}e$ is the only annihilation channel present.

The posteriors are consistent with the non-interacting DM scenario. The upper limits on P_{ann} , as obtained in the presence of σ_{drag} , have been used to infer upper limits on the strengths of the effective operators describing the relevant DM-electron interactions. The constraints on effective interactions are stringent; in particular, for $2m_e \lesssim m_\chi \lesssim \mathcal{O}(10)$ MeV these dominate over the constraints on the same lagrangian parameters, as inferred from the direct (and indirect) detection experiments [35, 137, 139–141].

Acknowledgements

RD thanks CSIR, India for financial support through Senior Research Fellowship (File no. 09/ 1128 (13346)/ 2022 EMR-I) and Shiv Nadar IoE (Deemed to be University). AP thanks the Indo-French Centre for the Promotion of Advanced Research for supporting the post-doctoral fellowship through the proposal 6704-4 under the Collaborative Scientific Research Programme. The authors gratefully acknowledge Kimberly Boddy and Vera Gluscevic for initial discussions regarding the code.

A The Collisional Boltzmann Equation

We consider the situation where the only relevant process for DM is its 2-to-2 scattering with electrons and annihilation of dark matter to an electron-positron pair. The evolution of the distribution functions is determined by the Boltzmann equation [145].

$$\frac{df_\chi}{d\lambda} = C_{\chi e \leftrightarrow \chi e}[p] + C_{\chi \bar{\chi} \leftrightarrow \bar{e} e}[p] \quad (\text{A.1})$$

where, f_χ is the distribution function for the evolution of dark matter.

$$\frac{\partial f_\chi}{\partial \tau} + \frac{p}{b} \hat{p}^i \frac{\partial f_\chi}{\partial x^i} + p \frac{\partial f_\chi}{\partial p} \left[-H + \frac{\partial \phi}{\partial \tau} - \frac{E}{p} \hat{p}^i \frac{\partial \psi}{\partial x^i} \right] = \frac{a}{E_\chi} (1 + \psi) (C_{\chi e \leftrightarrow \chi e}[p] + C_{\chi \bar{\chi} \leftrightarrow \bar{e} e}[p])$$

We need an equation for its bulk velocity. We multiply both side by v_χ and integrate over all v_χ . In non relativistic limits $E_\chi \simeq m_\chi$

$$\begin{aligned} & \int v_\chi \frac{d^3 v_\chi}{(2\pi)^3} \left[\frac{\partial f_\chi}{\partial \tau} + \frac{p}{E} \hat{p}^i \frac{\partial f_\chi}{\partial x^i} + p \frac{\partial f_\chi}{\partial p} \left(-\mathcal{H} + \frac{\partial \phi}{\partial \tau} - \frac{E}{p} \hat{p}^i \frac{\partial \psi}{\partial x^i} \right) \right] \\ &= \int v_\chi \frac{d^3 v_\chi}{(2\pi)^3} \left(\frac{a}{m_\chi} (1 + \psi) (C_{\chi e \leftrightarrow \chi e}[p] + C_{\chi \bar{\chi} \leftrightarrow \bar{e} e}[p]) \right) \end{aligned} \quad (\text{A.2})$$

Solving L.H.S gives

$$\frac{\partial}{\partial \tau} \left(n_\chi^{(0)} v_\chi \right) + \nabla \left[\frac{\delta p_\chi}{m_\chi} \right] + 4\mathcal{H} n_\chi^{(0)} v_\chi \quad (\text{A.3})$$

$\delta p_\chi = c_\chi^2 \delta \rho_\chi = c_\chi^2 n_\chi^{(0)} m_\chi \delta_\chi$, where c_χ^2 is the dark matter sound speed squared. Using particle conservation and following ref. [145] we get left side to be:

$$\frac{\partial \vec{V}_\chi}{\partial \tau} + c_\chi^2 \vec{\nabla} \delta_\chi + \frac{\dot{a}}{a} \vec{V}_\chi \quad (\text{A.4})$$

where V_χ is the peculiar velocity of the DM.

Both annihilation and scattering are governed by the same operators, but since scattering (or drag) dominates the effect in perturbation, and the effect of annihilation mainly comes from changes in the free electron fraction x_e , we can ignore annihilation for now. While annihilation can impact perturbations in some cases, it is not within the scope of this work.

A.1 Momentum transfer for DM-electron scattering

In C.O.M frame (For single collision)

$$\begin{aligned}
\vec{v}_{\chi,c} &= \vec{v}_\chi - \vec{v}_{\text{cm}} \\
\vec{v}_{\text{cm}} &= \frac{m_\chi \vec{v}_\chi + m_b \vec{v}_b}{m_\chi + m_b} \\
\vec{v}_{\chi,c} &= \vec{v}_\chi - \left(\frac{m_\chi \vec{v}_\chi + m_b \vec{v}_b}{m_\chi + m_b} \right) \\
\vec{v}_{\chi,c} &= \frac{m_b \vec{v}_\chi - m_b \vec{v}_b}{m_\chi + m_b} \\
\vec{v}_{\chi,c} &= \frac{m_b (\vec{v}_\chi - \vec{v}_b)}{m_\chi + m_b}
\end{aligned}$$

Velocity Exchange if after collision dark matter moves in \hat{n} direction C.O.M frame

$$\begin{aligned}
\Delta v_\chi &= \vec{v}'_{\chi,f} - \vec{v}_{\chi,c} \\
\Delta v_\chi &= \frac{m_b |\vec{v}_\chi - \vec{v}_b| \hat{n} - m_b (\vec{v}_\chi - \vec{v}_b)}{m_\chi + m_b}
\end{aligned}$$

Here $\vec{v}_{\chi,c}$ and $\vec{v}'_{\chi,c}$ refers to dark matter velocity after scattering before and after scattering in C.O.M frame.

$$\begin{aligned}
\Delta v_\chi &= \frac{m_b}{m_\chi + m_b} (|\vec{v}_\chi - \vec{v}_b| \hat{n} - (\vec{v}_\chi - \vec{v}_b)) \\
\Delta v_\chi &= \frac{m_b}{m_\chi + m_b} |\vec{v}_\chi - \vec{v}_b| \left(\hat{n} - \frac{(\vec{v}_\chi - \vec{v}_b)}{|\vec{v}_\chi - \vec{v}_b|} \right)
\end{aligned}$$

In non-relativistic limit, $\Delta P_\chi = m_\chi \Delta v_\chi$

$$\Delta P_\chi = \frac{m_\chi m_b}{m_\chi + m_b} |\vec{v}_\chi - \vec{v}_b| \left(\hat{n} - \frac{(\vec{v}_\chi - \vec{v}_b)}{|\vec{v}_\chi - \vec{v}_b|} \right) \quad (\text{A.5})$$

A.2 Drag from DM-Electron Scattering

The collision term in the Boltzmann equation for DM with initial velocity v_χ scattering with a baryon with initial velocity v_b , resulting in the final velocities v'_χ and v'_b , respectively.

$$\begin{aligned}
C_{\chi e \leftrightarrow \chi e}[p] &= \frac{1}{m_\chi} \iiint |M|^2 \times (2\pi)^4 \delta^4(P_\chi + P_b - P'_\chi - P'_b) \cdot \frac{d^3 v_b}{(2\pi)^3} \frac{d^3 v'_\chi}{(2\pi)^3} \frac{d^3 v'_b}{(2\pi)^3} \\
&\quad \times \{ f_b(v'_b) f_\chi(v'_\chi) [1 - f_\chi(v_\chi)] [1 - f_b(v_b)] - f_\chi(v_\chi) f_b(v_b) [1 - f_\chi(v'_\chi)] [1 - f_b(v'_b)] \}
\end{aligned} \quad (\text{A.6})$$

For fermionic dark matter and baryons, the collision integral simplifies to:

$$\begin{aligned}
C_{\chi e \leftrightarrow \chi e}[p] &= \frac{1}{m_\chi} \iiint |M|^2 \times \delta^4(P_\chi + P_b - P'_\chi - P'_b) \cdot \frac{d^3 v_b}{(2\pi)^3} \frac{d^3 v'_\chi}{(2\pi)^3} \frac{d^3 v'_b}{(2\pi)^3} \\
&\quad \times \{ f'_b f'_\chi - f_\chi f_b \}
\end{aligned} \quad (\text{A.7})$$

Here, $f'_b = f_b(v'_b)$, $f'_\chi = f_\chi(v'_\chi)$, $f_\chi = f_\chi(v_\chi)$, and $f_b = f_b(v_b)$.

The collision integral can be expressed in terms of the differential cross-section $\frac{d\sigma}{d\Omega}$:

$$\begin{aligned}
C_{\chi e \leftrightarrow \chi e}[p] &= \frac{1}{m_\chi} \int \frac{d^3 v_\chi}{(2\pi)^3} \int \frac{d^3 v_b}{(2\pi)^3} \int d\Omega \left(\frac{d\sigma}{d\Omega} \right) |\vec{v}_\chi - \vec{v}_b| f'_\chi f'_b \\
&\quad - \frac{1}{m_\chi} \int \frac{d^3 v_\chi}{(2\pi)^3} \int \frac{d^3 v_b}{(2\pi)^3} \int d\Omega \left(\frac{d\sigma}{d\Omega} \right) |\vec{v}_\chi - \vec{v}_b| f_\chi f_b
\end{aligned} \tag{A.8}$$

The momentum transfer term for is given by:

$$\begin{aligned}
\int v_\chi C[f] \frac{d^3 v_\chi}{(2\pi)^3} &= \frac{1}{m_\chi} \int (v'_\chi - \Delta v_\chi) \frac{d^3 v_\chi}{(2\pi)^3} \int \frac{d^3 v_b}{(2\pi)^3} \int d\Omega \left(\frac{d\sigma}{d\Omega} \right) |\vec{v}_\chi - \vec{v}_b| f'_\chi f'_b \\
&\quad - \frac{1}{m_\chi} \int \vec{v}_\chi \frac{d^3 v_\chi}{(2\pi)^3} \int \frac{d^3 v_b}{(2\pi)^3} \int d\Omega \left(\frac{d\sigma}{d\Omega} \right) |\vec{v}_\chi - \vec{v}_b| f_\chi f_b
\end{aligned} \tag{A.9}$$

This simplifies to:

$$\int v_\chi C[f] \frac{d^3 v_\chi}{(2\pi)^3} = -\frac{1}{m_\chi} \int \Delta v_\chi \frac{d^3 v_\chi}{(2\pi)^3} \int \frac{d^3 v_b}{(2\pi)^3} \int d\Omega \left(\frac{d\sigma}{d\Omega} \right) |\vec{v}_\chi - \vec{v}_b| \tag{A.10}$$

If there are n_b scattering centers, the momentum transfer becomes:

$$\begin{aligned}
\int v_\chi C[f] \frac{d^3 v_\chi}{(2\pi)^3} &= -\frac{n_b}{m_\chi} \int \frac{d^3 v_\chi}{(2\pi)^3} f_\chi \int \frac{d^3 v_b}{(2\pi)^3} f_b \\
&\quad \times \int d\Omega \left(\frac{d\sigma}{d\Omega} \right) |\vec{v}_\chi - \vec{v}_b| \Delta \vec{P}_\chi
\end{aligned}$$

Substituting the momentum transfer cross-section and simplifying:

$$\begin{aligned}
\int v_\chi C[f] \frac{d^3 v_\chi}{(2\pi)^3} &= \frac{\rho_b}{m_\chi + m_b} \int \frac{d^3 v_\chi}{(2\pi)^3} f_\chi \int \frac{d^3 v_b}{(2\pi)^3} f_b \int d\Omega \left(\frac{d\sigma}{d\Omega} \right) |\vec{v}_\chi - \vec{v}_b|^2 \\
&\quad \times \left(\hat{n} - \frac{(\vec{v}_\chi - \vec{v}_b)}{|\vec{v}_\chi - \vec{v}_b|} \right)
\end{aligned} \tag{A.11}$$

The distribution functions for dark matter (f_χ) and baryons (f_b) are given by:

$$\begin{aligned}
f_\chi(\vec{v}_\chi) &= \frac{1}{(2\pi)^3 \bar{v}_\chi^3} \exp \left[-\frac{(\vec{v}_\chi - \vec{V}_\chi)^2}{2\bar{v}_\chi^2} \right], \\
f_b(\vec{v}_b) &= \frac{1}{(2\pi)^3 \bar{v}_b^3} \exp \left[-\frac{(\vec{v}_b - \vec{V}_b)^2}{2\bar{v}_b^2} \right],
\end{aligned}$$

where $\bar{v}_\chi^2 = T_\chi/m_\chi$ and $\bar{v}_b^2 = T_b/m_b$ are the thermal velocity dispersions.

To simplify calculations, we introduce new variables:

$$\begin{aligned}
\vec{v}_m &\equiv \frac{\bar{v}_b^2 \vec{v}_\chi + \bar{v}_\chi^2 \vec{v}_b}{\bar{v}_b^2 + \bar{v}_\chi^2}, \\
\vec{v}_r &\equiv \vec{v}_\chi - \vec{v}_b.
\end{aligned}$$

With these new variables, the distribution functions remain factorizable:

$$\int d^3v_\chi f_\chi(\vec{v}_\chi) \int d^3v_b f_b(\vec{v}_b) = \int d^3v_r f_r(\vec{v}_r) \int d^3v_m f_m(\vec{v}_m).$$

The new distribution functions f_m and f_r are Gaussian:

$$f_m(\vec{v}_m) = \frac{1}{(2\pi)^3 \bar{v}_m^3} \exp\left[-\frac{(\vec{v}_m - \vec{V}_m)^2}{2\bar{v}_m^2}\right], \quad f_r(\vec{v}_r) = \frac{1}{(2\pi)^3 \bar{v}_r^3} \exp\left[-\frac{(\vec{v}_r - \vec{V}_r)^2}{2\bar{v}_r^2}\right],$$

where:

$$\vec{V}_m = \frac{\bar{v}_b^2 \vec{V}_\chi + \bar{v}_\chi^2 \vec{V}_b}{\bar{v}_b^2 + \bar{v}_\chi^2}, \quad \bar{v}_m^2 = \frac{\bar{v}_\chi^2 \bar{v}_b^2}{\bar{v}_\chi^2 + \bar{v}_b^2}$$

$$\vec{V}_r = \vec{V}_\chi - \vec{V}_b, \quad \bar{v}_r^2 = \bar{v}_\chi^2 + \bar{v}_b^2.$$

V_χ and V_b are the peculiar velocity of the DM and the baryon. In this work we are interested in the interaction of a DM-electron, so we now replace b with e for the electron.

$$\int v_\chi C[f] \frac{d^3v_\chi}{(2\pi)^3} = -\frac{Y_b \rho_e \sigma_{\text{drag}}}{m_\chi + m_e} \int \frac{d^3v_r}{(2\pi)^3} f_r(\vec{v}_r) v_r^{n+1} \vec{v}_r \int \frac{d^3v_m}{(2\pi)^3} v_m f_m(\vec{v}_m) \quad (\text{A.12})$$

where we obtain the second line by completing the integration over angles to obtain the momentum-transfer cross section and by utilizing. The integral over \vec{v}_m simply evaluates to 1, and the remaining integral over \vec{v}_r yields the result

$$\int v_\chi C[f] \frac{d^3v_\chi}{(2\pi)^3} = -\frac{Y_b \rho_e \sigma_{\text{drag}} \mathcal{N}_n}{m_\chi + m_e} \bar{v}_r^{n+1} \vec{v}_r, {}_1F_1\left(-\frac{n+1}{2}, \frac{5}{2}, -\frac{r^2}{2}\right).$$

using Eq. [A.4]

$$\frac{\partial \vec{V}_\chi}{\partial \tau} + c_\chi^2 \vec{\nabla} \delta_\chi + \frac{\dot{a}}{a} \vec{V}_\chi = -a Y_b \rho_e \sigma_{\text{drag}} \frac{\mathcal{N}_n}{m_\chi + m_e} \bar{v}_r^{n+1} \vec{v}_r, {}_1F_1\left(-\frac{n+1}{2}, \frac{5}{2}, -\frac{r^2}{2}\right) \quad (\text{A.13})$$

Taking divergence $\nabla \cdot$, both side then in k space above equation can be written as

$$\dot{\theta}_\chi + \mathcal{H} \theta_\chi - c_\chi^2 k^2 \delta_\chi = R_\chi (\theta_b - \theta_\chi)$$

where

$$R_\chi = a Y_b \rho_e \sigma_{\text{drag}} \frac{\mathcal{N}_n}{m_\chi + m_e} \bar{v}_r^{n+1} {}_1F_1\left(-\frac{n+1}{2}, \frac{5}{2}, -\frac{r^2}{2}\right) \quad (\text{A.14})$$

Here, the relative velocity is given by

$$\bar{v}_r = \left(\frac{T_b}{m_e} + \frac{T_\chi}{m_\chi} + \frac{V_{\text{rms}}^2}{3} \right)^{1/2}. \quad (\text{A.15})$$

where $V_{\text{rms}}^2 = \langle \vec{V}_\chi^2 \rangle_\xi = \int \frac{dk}{k} \Delta_\xi \left(\frac{\theta_b - \theta_c}{k} \right)^2$ and $\langle \dots \rangle_\xi$ denotes an average with respect to the primordial curvature perturbation, and $\Delta_\xi \simeq 2.4 \times 10^{-9}$ is the primordial curvature variance per log k [122].

For $n \geq 0$, the root mean square (r.m.s.) velocity is zero, i.e., $V_{\text{r.m.s}} = 0$. Since we are primarily interested in velocity-independent scattering cross sections in this work, the expression simplifies to $\bar{v}_r = \left(\frac{T_b}{m_e} + \frac{T_\chi}{m_\chi} \right)^{1/2}$.

B Cross-section for Annihilation and Scattering

Assuming both dark matter and electrons are non-relativistic, the differential dark matter-electron scattering cross section is given by:

$$\frac{d\sigma_{\text{drag}}}{d\cos\theta_*} = \frac{|\overline{\mathcal{M}}|_{sc}^2}{32\pi(m_e + m_\chi)^2}$$

$$\sigma_{\text{drag}} = \int \frac{|\overline{\mathcal{M}}|_{sc}^2}{32\pi(m_e + m_\chi)^2} d\cos\theta_* \quad (\text{B.1})$$

where $|\overline{\mathcal{M}}|_{sc}^2$ is the spin-averaged amplitude squared of dark matter-baryon scattering and σ_{drag} is the cross-section of DM-e scattering.

Similarly, for dark matter annihilation to electron cross section is given by :

$$\frac{d\sigma_{\text{ann}}}{d\cos\theta_*} = \frac{|\overline{\mathcal{M}}|_{\text{ann}}^2}{16\pi v_{\chi,rel} s} \sqrt{1 - \frac{m_e^2}{m_\chi^2}} \quad (\text{B.2})$$

where $|\overline{\mathcal{M}}|_{\text{ann}}^2$ is the spin-averaged amplitude squared for dark matter annihilation into electrons. The Mandelstam variable s is defined in the center-of-mass (c.o.m.) frame as

$$s \simeq 4m_\chi^2 + m_\chi^2 v_{\chi,rel}^2$$

where v is the relative velocity of the annihilating DM particles.

First, we will try to solve the Axial-Vector operator for Dark Matter Electron interaction.

$$\mathcal{L} = g_{eff} \bar{\psi} \gamma^\mu \gamma^5 \psi \bar{e} \gamma_\mu \gamma^5 e$$

Eqs. [B.1] and [B.2] gives the cross-section for dark matter scattering and annihilation as:

$$\sigma_{\text{drag}} = g_{\text{eff}}^2 \frac{3}{4} \left(\frac{16m_e^2}{\pi \left(1 + \frac{m_e}{m_\psi}\right)^2} \right) \quad (\text{B.3})$$

and,

$$\langle \sigma v_{\chi,rel} \rangle = \frac{1}{2\pi} g_{\text{eff}}^2 m_\psi^2 \left(\sqrt{1 - \frac{m_e^2}{m_\psi^2}} \right) \left[\frac{m_e^2}{m_\psi^2} + \frac{1}{12} \left(2 - \frac{m_e^2}{m_\psi^2} \right) v_{\chi,rel}^2 \right] \quad (\text{B.4})$$

Similarly, for the Vector operator

$$\mathcal{L} = g_{\text{eff}} \bar{\psi} \gamma^\mu \psi \bar{e} \gamma_\mu e$$

Eqs. [B.1] and [B.2] gives the cross-section for dark matter scattering and annihilation as:

$$\sigma_{\text{drag}} = \frac{g_{\text{eff}}^2 \mu^2}{\pi} \quad (\text{B.5})$$

and,

$$\langle \sigma v_{\chi, \text{rel}} \rangle = g_{\text{eff}}^2 \frac{m_{\psi}^2}{2\pi} \sqrt{1 - \frac{m_e^2}{m_{\psi}^2}} \times \left[\left(2 + \frac{m_e^2}{m_{\psi}^2} \right) \right] \quad (\text{B.6})$$

For Tensor operator

$$\mathcal{L} = g_{\text{eff}} \bar{\psi} \sigma^{\mu\nu} \psi \bar{e} \sigma_{\mu\nu} e$$

again following the same process the cross-section for dark matter scattering and annihilation for the above tensor operator as:

$$\sigma_{\text{drag}} = \frac{48 \times \mu^2 g_{\text{eff}}^2}{\pi} \quad (\text{B.7})$$

and,

$$\langle \sigma v_{\chi, \text{rel}} \rangle = g_{\text{eff}}^2 \frac{m_{\psi}^2}{2\pi} \sqrt{1 - \frac{m_e^2}{m_{\psi}^2}} \times \left[16 \left(1 + \frac{m_e^2}{m_{\psi}^2} \right) \right]. \quad (\text{B.8})$$

where μ is reduced mass for dark matter and electron system. These equations can also be checked from [124, 146].

For the scalar operator, the interaction lagrangian is:

$$\mathcal{L} = g_{\text{eff}} \phi^\dagger \phi \bar{e} e$$

Using Eqs. [B.1] and [B.2], the cross-section for dark matter scattering and annihilation is:

$$\sigma_{\text{drag}} = \frac{g_{\text{eff}}^2}{16\pi \left(1 + \frac{m_\phi}{m_e} \right)^2} \quad (\text{B.9})$$

and,

$$\langle \sigma v_{\chi, \text{rel}} \rangle = g_{\text{eff}}^2 \frac{1}{8\pi} \left(1 - \frac{m_e^2}{m_\phi^2} \right)^{\frac{3}{2}} \quad (\text{B.10})$$

where $\mu = \frac{m_e m_\phi}{m_e + m_\phi}$ is the reduced mass of the dark matter-electron system.

References

- [1] **Planck** Collaboration, P. A. R. Ade *et al.*, “Planck 2015 results. XIII. Cosmological parameters,” *Astron. Astrophys.* **594** (2016) A13, [arXiv:1502.01589 \[astro-ph.CO\]](#).
- [2] **Planck** Collaboration, N. Aghanim *et al.*, “Planck 2018 results. VI. Cosmological parameters,” *Astron. Astrophys.* **641** (2020) A6, [arXiv:1807.06209 \[astro-ph.CO\]](#).
- [3] G. Bertone, D. Hooper, and J. Silk, “Particle dark matter: Evidence, candidates and constraints,” *Phys. Rept.* **405** (2005) 279–390, [arXiv:hep-ph/0404175](#).
- [4] G. Jungman, M. Kamionkowski, and K. Griest, “Supersymmetric dark matter,” *Phys. Rept.* **267** (1996) 195–373, [arXiv:hep-ph/9506380](#).
- [5] M. Cirelli, A. Strumia, and J. Zupan, “Dark Matter,” [arXiv:2406.01705 \[hep-ph\]](#).
- [6] E. W. Kolb, *The Early Universe*, vol. 69. Taylor and Francis, 5, 2019.
- [7] **PICO** Collaboration, C. Amole *et al.*, “Dark Matter Search Results from the Complete Exposure of the PICO-60 C₃F₈ Bubble Chamber,” *Phys. Rev. D* **100** no. 2, (2019) 022001, [arXiv:1902.04031 \[astro-ph.CO\]](#).
- [8] T. Emken, R. Essig, C. Kouvaris, and M. Sholapurkar, “Direct Detection of Strongly Interacting Sub-GeV Dark Matter via Electron Recoils,” *JCAP* **09** (2019) 070, [arXiv:1905.06348 \[hep-ph\]](#).
- [9] **PandaX-II** Collaboration, Q. Wang *et al.*, “Results of dark matter search using the full PandaX-II exposure,” *Chin. Phys. C* **44** no. 12, (2020) 125001, [arXiv:2007.15469 \[astro-ph.CO\]](#).
- [10] **LZ** Collaboration, J. Aalbers *et al.*, “First Dark Matter Search Results from the LUX-ZEPLIN (LZ) Experiment,” *Phys. Rev. Lett.* **131** no. 4, (2023) 041002, [arXiv:2207.03764 \[hep-ex\]](#).
- [11] **XENON** Collaboration, E. Aprile *et al.*, “First Dark Matter Search with Nuclear Recoils from the XENONnT Experiment,” *Phys. Rev. Lett.* **131** no. 4, (2023) 041003, [arXiv:2303.14729 \[hep-ex\]](#).
- [12] **IceCube** Collaboration, R. Abbasi *et al.*, “Search for GeV-scale dark matter annihilation in the Sun with IceCube DeepCore,” *Phys. Rev. D* **105** no. 6, (2022) 062004, [arXiv:2111.09970 \[astro-ph.HE\]](#).
- [13] **Fermi-LAT**, **DES** Collaboration, A. Albert *et al.*, “Searching for Dark Matter Annihilation in Recently Discovered Milky Way Satellites with Fermi-LAT,” *Astrophys. J.* **834** no. 2, (2017) 110, [arXiv:1611.03184 \[astro-ph.HE\]](#).
- [14] **Fermi-LAT** Collaboration, M. Ackermann *et al.*, “Searching for Dark Matter Annihilation from Milky Way Dwarf Spheroidal Galaxies with Six Years of Fermi Large Area Telescope Data,” *Phys. Rev. Lett.* **115** no. 23, (2015) 231301, [arXiv:1503.02641 \[astro-ph.HE\]](#).
- [15] **MAGIC**, **Fermi-LAT** Collaboration, M. L. Ahnen *et al.*, “Limits to Dark Matter Annihilation Cross-Section from a Combined Analysis of MAGIC and Fermi-LAT Observations of Dwarf Satellite Galaxies,” *JCAP* **02** (2016) 039, [arXiv:1601.06590 \[astro-ph.HE\]](#).
- [16] M. Regis *et al.*, “The EMU view of the Large Magellanic Cloud: troubles for sub-TeV WIMPs,” *JCAP* **11** no. 11, (2021) 046, [arXiv:2106.08025 \[astro-ph.HE\]](#).
- [17] O. Adriani *et al.*, “Measurement of the flux of primary cosmic ray antiprotons with energies of 60-MeV to 350-GeV in the PAMELA experiment,” *Pisma Zh. Eksp. Teor. Fiz.* **96** (2012) 693–699.
- [18] O. Adriani *et al.*, “A new measurement of the antiproton-to-proton flux ratio up to 100 GeV in the cosmic radiation,” *Phys. Rev. Lett.* **102** (2009) 051101, [arXiv:0810.4994 \[astro-ph\]](#).

- [19] **AMS Collaboration**, M. Aguilar *et al.*, “Antiproton Flux, Antiproton-to-Proton Flux Ratio, and Properties of Elementary Particle Fluxes in Primary Cosmic Rays Measured with the Alpha Magnetic Spectrometer on the International Space Station,” *Phys. Rev. Lett.* **117** no. 9, (2016) 091103, [arXiv:1612.09579 \[astro-ph.HE\]](#).
- [20] **AMS-02 Collaboration**, S. Caroff, “High Statistics Measurement of the Positron Fraction in Primary Cosmic Rays with the Alpha Magnetic Spectrometer on the International Space Station,” in *25th European Cosmic Ray Symposium*. 12, 2016. [arXiv:1612.09579 \[astro-ph.HE\]](#).
- [21] **AMS Collaboration** Collaboration, M. Aguilar and Aisa, “Precision measurement of the ($e^+ + e^-$) flux in primary cosmic rays from 0.5 gev to 1 tev with the alpha magnetic spectrometer on the international space station,” *Phys. Rev. Lett.* **113** (Nov, 2014) 221102.
- [22] **AMS-02 Collaboration**, M. Vecchi, “Precision measurement of the ($e^+ + e^-$) flux in primary cosmic rays from 0.5 GeV to 1 TeV with the Alpha Magnetic Spectrometer on the International Space Station,” in *25th European Cosmic Ray Symposium*. 1, 2017. [arXiv:1701.02212 \[astro-ph.HE\]](#).
- [23] M. Cirelli, N. Fornengo, J. Koechler, E. Pinetti, and B. M. Roach, “Putting all the X in one basket: Updated X-ray constraints on sub-GeV Dark Matter,” *JCAP* **07** (2023) 026, [arXiv:2303.08854 \[hep-ph\]](#).
- [24] **CMS Collaboration**, A. Hayrapetyan *et al.*, “Dark sector searches with the CMS experiment,” [arXiv:2405.13778 \[hep-ex\]](#).
- [25] **ATLAS Collaboration**, M. Aaboud *et al.*, “Search for an invisibly decaying Higgs boson or dark matter candidates produced in association with a Z boson in pp collisions at $\sqrt{s} = 13$ TeV with the ATLAS detector,” *Phys. Lett. B* **776** (2018) 318–337, [arXiv:1708.09624 \[hep-ex\]](#).
- [26] **CMS Collaboration**, A. Hayrapetyan *et al.*, “Search for Inelastic Dark Matter in Events with Two Displaced Muons and Missing Transverse Momentum in Proton-Proton Collisions at $s=13$ TeV,” *Phys. Rev. Lett.* **132** no. 4, (2024) 041802, [arXiv:2305.11649 \[hep-ex\]](#).
- [27] **ATLAS Collaboration**, G. Aad *et al.*, “Search for new particles in events with a hadronically decaying W or Z boson and large missing transverse momentum at $\sqrt{s} = 13$ TeV using the ATLAS detector,” [arXiv:2406.01272 \[hep-ex\]](#).
- [28] **ATLAS Collaboration**, G. Aad *et al.*, “Search for dark matter produced in association with a dark Higgs boson in the $b\bar{b}$ final state using pp collisions at $\sqrt{s} = 13$ TeV with the ATLAS detector,” [arXiv:2407.10549 \[hep-ex\]](#).
- [29] **ATLAS Collaboration**, G. Aad *et al.*, “Search for new phenomena in events with an energetic jet and missing transverse momentum in pp collisions at $\sqrt{s} = 13$ TeV with the ATLAS detector,” *Phys. Rev. D* **103** no. 11, (2021) 112006, [arXiv:2102.10874 \[hep-ex\]](#).
- [30] **ATLAS Collaboration**, G. Aad *et al.*, “Search for dark matter in association with an energetic photon in pp collisions at $\sqrt{s} = 13$ TeV with the ATLAS detector,” *JHEP* **02** (2021) 226, [arXiv:2011.05259 \[hep-ex\]](#).
- [31] **ATLAS Collaboration**, “Measuring the b -jet identification efficiency for high p_T jets using multijet events in proton–proton collisions at $\sqrt{s} = 13$ TeV recorded with the ATLAS detector.”.
- [32] R. Essig, A. Manalaysay, J. Mardon, P. Sorensen, and T. Volansky, “First Direct Detection Limits on sub-GeV Dark Matter from XENON10,” *Phys. Rev. Lett.* **109** (2012) 021301, [arXiv:1206.2644 \[astro-ph.CO\]](#).
- [33] R. Essig, T. Volansky, and T.-T. Yu, “New Constraints and Prospects for sub-GeV Dark Matter Scattering off Electrons in Xenon,” *Phys. Rev. D* **96** no. 4, (2017) 043017, [arXiv:1703.00910 \[hep-ph\]](#).

- [34] **SENSEI** Collaboration, O. Abramoff *et al.*, “SENSEI: Direct-Detection Constraints on Sub-GeV Dark Matter from a Shallow Underground Run Using a Prototype Skipper-CCD,” *Phys. Rev. Lett.* **122** no. 16, (2019) 161801, [arXiv:1901.10478 \[hep-ex\]](#).
- [35] **SENSEI** Collaboration, L. Barak *et al.*, “SENSEI: Direct-Detection Results on sub-GeV Dark Matter from a New Skipper-CCD,” *Phys. Rev. Lett.* **125** no. 17, (2020) 171802, [arXiv:2004.11378 \[astro-ph.CO\]](#).
- [36] Y. Kahn and T. Lin, “Searches for light dark matter using condensed matter systems,” *Rept. Prog. Phys.* **85** no. 6, (2022) 066901, [arXiv:2108.03239 \[hep-ph\]](#).
- [37] **DarkSide** Collaboration, P. Agnes *et al.*, “Constraints on Sub-GeV Dark-Matter Electron Scattering from the DarkSide-50 Experiment,” *Phys. Rev. Lett.* **121** no. 11, (2018) 111303, [arXiv:1802.06998 \[astro-ph.CO\]](#).
- [38] G. Zaharijas and G. R. Farrar, “A Window in the dark matter exclusion limits,” *Phys. Rev. D* **72** (2005) 083502, [arXiv:astro-ph/0406531](#).
- [39] T. Emken and C. Kouvaris, “DaMaSCUS: The Impact of Underground Scatterings on Direct Detection of Light Dark Matter,” *JCAP* **10** (2017) 031, [arXiv:1706.02249 \[hep-ph\]](#).
- [40] M. S. Mahdawi and G. R. Farrar, “Closing the window on \sim GeV Dark Matter with moderate ($\sim \mu\text{b}$) interaction with nucleons,” *JCAP* **12** (2017) 004, [arXiv:1709.00430 \[hep-ph\]](#).
- [41] F. Hasenbalg, D. Abriola, F. T. Avignone, J. I. Collar, D. E. Di Gregorio, A. O. Gattone, H. Huck, D. Tomasi, and I. Urteaga, “Cold dark matter identification: Diurnal modulation revisited,” *Phys. Rev. D* **55** (1997) 7350–7355, [arXiv:astro-ph/9702165](#).
- [42] S. K. Lee, M. Lisanti, S. Mishra-Sharma, and B. R. Safdi, “Modulation Effects in Dark Matter-Electron Scattering Experiments,” *Phys. Rev. D* **92** no. 8, (2015) 083517, [arXiv:1508.07361 \[hep-ph\]](#).
- [43] T. Emken, C. Kouvaris, and I. M. Shoemaker, “Terrestrial Effects on Dark Matter-Electron Scattering Experiments,” *Phys. Rev. D* **96** no. 1, (2017) 015018, [arXiv:1702.07750 \[hep-ph\]](#).
- [44] N. Padmanabhan and D. P. Finkbeiner, “Detecting dark matter annihilation with CMB polarization: Signatures and experimental prospects,” *Phys. Rev. D* **72** (2005) 023508, [arXiv:astro-ph/0503486](#).
- [45] T. R. Slatyer, N. Padmanabhan, and D. P. Finkbeiner, “CMB Constraints on WIMP Annihilation: Energy Absorption During the Recombination Epoch,” *Phys. Rev. D* **80** (2009) 043526, [arXiv:0906.1197 \[astro-ph.CO\]](#).
- [46] S. Galli, F. Iocco, G. Bertone, and A. Melchiorri, “CMB constraints on Dark Matter models with large annihilation cross-section,” *Phys. Rev. D* **80** (2009) 023505, [arXiv:0905.0003 \[astro-ph.CO\]](#).
- [47] L. Lopez-Honorez, O. Mena, S. Palomares-Ruiz, and A. C. Vincent, “Constraints on dark matter annihilation from CMB observations before Planck,” *JCAP* **07** (2013) 046, [arXiv:1303.5094 \[astro-ph.CO\]](#).
- [48] C. Dvorkin, K. Blum, and M. Zaldarriaga, “Perturbed Recombination from Dark Matter Annihilation,” *Phys. Rev. D* **87** no. 10, (2013) 103522, [arXiv:1302.4753 \[astro-ph.CO\]](#).
- [49] G. Giesen, J. Lesgourgues, B. Audren, and Y. Ali-Haïmoud, “CMB photons shedding light on dark matter,” *JCAP* **12** (2012) 008, [arXiv:1209.0247 \[astro-ph.CO\]](#).
- [50] T. R. Slatyer, “Indirect dark matter signatures in the cosmic dark ages. I. Generalizing the bound on s-wave dark matter annihilation from Planck results,” *Phys. Rev. D* **93** no. 2, (2016) 023527, [arXiv:1506.03811 \[hep-ph\]](#).

- [51] D. Green, P. D. Meerburg, and J. Meyers, “Aspects of Dark Matter Annihilation in Cosmology,” *JCAP* **04** (2019) 025, [arXiv:1804.01055 \[astro-ph.CO\]](#).
- [52] E. Bertschinger, “The Effects of Cold Dark Matter Decoupling and Pair Annihilation on Cosmological Perturbations,” *Phys. Rev. D* **74** (2006) 063509, [arXiv:astro-ph/0607319](#).
- [53] M. Kawasaki, H. Nakatsuka, K. Nakayama, and T. Sekiguchi, “Revisiting CMB constraints on dark matter annihilation,” *JCAP* **12** no. 12, (2021) 015, [arXiv:2105.08334 \[astro-ph.CO\]](#).
- [54] C. Dvorkin, K. Blum, and M. Kamionkowski, “Constraining Dark Matter-Baryon Scattering with Linear Cosmology,” *Phys. Rev. D* **89** no. 2, (2014) 023519, [arXiv:1311.2937 \[astro-ph.CO\]](#).
- [55] C. Dvorkin, K. Blum, and M. Kamionkowski, “Constraining Dark Matter-Baryon Scattering with Linear Cosmology,” *Phys. Rev. D* **89** no. 2, (2014) 023519, [arXiv:1311.2937 \[astro-ph.CO\]](#).
- [56] C. Dvorkin, K. Blum, and M. Kamionkowski, “Constraining dark matter-baryon scattering with linear cosmology,” *Physical Review D* **89** no. 2, (Jan, 2014) .
- [57] W. L. Xu, C. Dvorkin, and A. Chael, “Probing sub-GeV Dark Matter-Baryon Scattering with Cosmological Observables,” *Phys. Rev. D* **97** no. 10, (2018) 103530, [arXiv:1802.06788 \[astro-ph.CO\]](#).
- [58] V. Gluscevic and K. K. Boddy, “Constraints on Scattering of keV–TeV Dark Matter with Protons in the Early Universe,” *Phys. Rev. Lett.* **121** no. 8, (2018) 081301, [arXiv:1712.07133 \[astro-ph.CO\]](#).
- [59] K. K. Boddy and V. Gluscevic, “First Cosmological Constraint on the Effective Theory of Dark Matter-Proton Interactions,” *Phys. Rev. D* **98** no. 8, (2018) 083510, [arXiv:1801.08609 \[astro-ph.CO\]](#).
- [60] K. K. Boddy, V. Gluscevic, V. Poulin, E. D. Kovetz, M. Kamionkowski, and R. Barkana, “Critical assessment of CMB limits on dark matter-baryon scattering: New treatment of the relative bulk velocity,” *Phys. Rev. D* **98** no. 12, (2018) 123506, [arXiv:1808.00001 \[astro-ph.CO\]](#).
- [61] W. L. Xu, C. Dvorkin, and A. Chael, “Probing sub-GeV Dark Matter-Baryon Scattering with Cosmological Observables,” *Phys. Rev. D* **97** no. 10, (2018) 103530, [arXiv:1802.06788 \[astro-ph.CO\]](#).
- [62] C. Dvorkin, T. Lin, and K. Schutz, “Cosmology of Sub-MeV Dark Matter Freeze-In,” *Phys. Rev. Lett.* **127** no. 11, (2021) 111301, [arXiv:2011.08186 \[astro-ph.CO\]](#).
- [63] D. V. Nguyen, D. Sarnaik, K. K. Boddy, E. O. Nadler, and V. Gluscevic, “Observational constraints on dark matter scattering with electrons,” *Phys. Rev. D* **104** no. 10, (2021) 103521, [arXiv:2107.12380 \[astro-ph.CO\]](#).
- [64] K. K. Boddy, G. Krnjaic, and S. Moltner, “Investigation of CMB constraints for dark matter-helium scattering,” *Phys. Rev. D* **106** no. 4, (2022) 043510, [arXiv:2204.04225 \[astro-ph.CO\]](#).
- [65] Y. Ali-Haïmoud, S. S. Gandhi, and T. L. Smith, “Exact treatment of weak dark matter-baryon scattering for linear-cosmology observables,” *Phys. Rev. D* **109** no. 8, (2024) 083523, [arXiv:2312.08497 \[astro-ph.CO\]](#).
- [66] Y. Ali-Haïmoud, J. Chluba, and M. Kamionkowski, “Constraints on Dark Matter Interactions with Standard Model Particles from Cosmic Microwave Background Spectral Distortions,” *Phys. Rev. Lett.* **115** no. 7, (2015) 071304, [arXiv:1506.04745 \[astro-ph.CO\]](#).
- [67] J. Chluba, “Future Steps in Cosmology using Spectral Distortions of the Cosmic Microwave Background,” *Proc. Int. Sch. Phys. Fermi* **200** (2020) 265–309, [arXiv:1806.02915 \[astro-ph.CO\]](#).

- [68] Y. Ali-Haïmoud, “Testing dark matter interactions with CMB spectral distortions,” *Phys. Rev. D* **103** no. 4, (2021) 043541, [arXiv:2101.04070 \[astro-ph.CO\]](#).
- [69] R. J. Wilkinson, C. Boehm, and J. Lesgourgues, “Constraining dark matter-neutrino interactions using the cmb and large-scale structure,” *Journal of Cosmology and Astroparticle Physics* **2014** no. 05, (May, 2014) 011–011.
- [70] G. Mangano, A. Melchiorri, P. Serra, A. Cooray, and M. Kamionkowski, “Cosmological bounds on dark-matter-neutrino interactions,” *Physical Review D* **74** no. 4, (Aug, 2006) .
- [71] F. Forastieri, M. Lattanzi, and P. Natoli, “Constraints on secret neutrino interactions after Planck,” *JCAP* **1507** no. 07, (2015) 014, [arXiv:1504.04999 \[astro-ph.CO\]](#).
- [72] A. Paul, A. Chatterjee, A. Ghoshal, and S. Pal, “Shedding light on dark matter and neutrino interactions from cosmology,” *JCAP* **10** (2021) 017, [arXiv:2104.04760 \[hep-ph\]](#).
- [73] S. Ghosh, R. Khatri, and T. S. Roy, “Can dark neutrino interactions phase out the Hubble tension?,” *Phys. Rev. D* **102** no. 12, (2020) 123544, [arXiv:1908.09843 \[hep-ph\]](#).
- [74] L. Ackerman, M. R. Buckley, S. M. Carroll, and M. Kamionkowski, “Dark Matter and Dark Radiation,” *Phys. Rev. D* **79** (2009) 023519, [arXiv:0810.5126 \[hep-ph\]](#).
- [75] V. Poulin, J. L. Bernal, E. D. Kovetz, and M. Kamionkowski, “Sigma-8 tension is a drag,” *Phys. Rev. D* **107** no. 12, (2023) 123538, [arXiv:2209.06217 \[astro-ph.CO\]](#).
- [76] M. Lucca, “Dark energy–dark matter interactions as a solution to the S8 tension,” *Phys. Dark Univ.* **34** (2021) 100899, [arXiv:2105.09249 \[astro-ph.CO\]](#).
- [77] M. Mapelli, A. Ferrara, and E. Pierpaoli, “Impact of dark matter decays and annihilations on reionization,” *Mon. Not. Roy. Astron. Soc.* **369** (2006) 1719–1724, [arXiv:astro-ph/0603237](#).
- [78] M. Cirelli, F. Iocco, and P. Panci, “Constraints on Dark Matter annihilations from reionization and heating of the intergalactic gas,” *JCAP* **10** (2009) 009, [arXiv:0907.0719 \[astro-ph.CO\]](#).
- [79] M. Valdes, C. Evoli, and A. Ferrara, “Particle energy cascade in the intergalactic medium,” *Monthly Notices of the Royal Astronomical Society* **404** no. 3, (2010) 1569–1582, [arXiv:0911.1125 \[astro-ph.CO\]](#).
- [80] A. A. Kaurov, D. Hooper, and N. Y. Gnedin, “The Effects of Dark Matter Annihilation on Cosmic Reionization,” *Astrophys. J.* **833** no. 2, (2016) 162, [arXiv:1512.00526 \[astro-ph.CO\]](#).
- [81] T. R. Slatyer and C.-L. Wu, “Early-Universe constraints on dark matter-baryon scattering and their implications for a global 21 cm signal,” *Phys. Rev. D* **98** no. 2, (2018) 023013, [arXiv:1803.09734 \[astro-ph.CO\]](#).
- [82] H. Liu, T. R. Slatyer, and J. Zavala, “Contributions to cosmic reionization from dark matter annihilation and decay,” *Phys. Rev. D* **94** no. 6, (2016) 063507, [arXiv:1604.02457 \[astro-ph.CO\]](#).
- [83] T. R. Slatyer, “Indirect Dark Matter Signatures in the Cosmic Dark Ages II. Ionization, Heating and Photon Production from Arbitrary Energy Injections,” *Phys. Rev. D* **93** no. 2, (2016) 023521, [arXiv:1506.03812 \[astro-ph.CO\]](#).
- [84] J. B. Muñoz, E. D. Kovetz, and Y. Ali-Haïmoud, “Heating of Baryons due to Scattering with Dark Matter During the Dark Ages,” *Phys. Rev. D* **92** no. 8, (2015) 083528, [arXiv:1509.00029 \[astro-ph.CO\]](#).
- [85] M. Valdes, A. Ferrara, M. Mapelli, and E. Ripamonti, “Constraining DM through 21 cm observations,” *Mon. Not. Roy. Astron. Soc.* **377** (2007) 245–252, [arXiv:astro-ph/0701301](#).
- [86] J. A. Frieman, E. W. Kolb, and M. S. Turner, “Eternal annihilations: New constraints on long-lived particles from big-bang nucleosynthesis,” *Phys. Rev. D* **41** (May, 1990) 3080–3085.

- [87] K. Jedamzik, “Neutralinos and Big Bang nucleosynthesis,” *Phys. Rev. D* **70** (2004) 083510, [arXiv:astro-ph/0405583](#).
- [88] M. Kawasaki, K. Kohri, T. Moroi, and Y. Takaesu, “Revisiting Big-Bang Nucleosynthesis Constraints on Dark-Matter Annihilation,” *Phys. Lett. B* **751** (2015) 246–250, [arXiv:1509.03665 \[hep-ph\]](#).
- [89] P. F. Depta, M. Hufnagel, K. Schmidt-Hoberg, and S. Wild, “BBN constraints on the annihilation of MeV-scale dark matter,” *JCAP* **04** (2019) 029, [arXiv:1901.06944 \[hep-ph\]](#).
- [90] P. Braat and M. Hufnagel, “Big Bang Nucleosynthesis constraints on resonant DM annihilations,” *JCAP* **02** (2025) 032, [arXiv:2409.14900 \[hep-ph\]](#).
- [91] P.-H. Gu and X.-G. He, “Electrophilic dark matter with dark photon: from DAMPE to direct detection,” *Phys. Lett. B* **778** (2018) 292–295, [arXiv:1711.11000 \[hep-ph\]](#).
- [92] E. Di Valentino, C. Bøehm, E. Hivon, and F. R. Bouchet, “Reducing the H_0 and σ_8 tensions with Dark Matter-neutrino interactions,” *Phys. Rev.* **D97** no. 4, (2018) 043513, [arXiv:1710.02559 \[astro-ph.CO\]](#).
- [93] A. He, M. M. Ivanov, R. An, and V. Gluscevic, “ S_8 Tension in the Context of Dark Matter–Baryon Scattering,” *Astrophys. J. Lett.* **954** no. 1, (2023) L8, [arXiv:2301.08260 \[astro-ph.CO\]](#).
- [94] **KiDS** Collaboration, M. Asgari *et al.*, “KiDS-1000 Cosmology: Cosmic shear constraints and comparison between two point statistics,” *Astron. Astrophys.* **645** (2021) A104, [arXiv:2007.15633 \[astro-ph.CO\]](#).
- [95] H. Hildebrandt *et al.*, “KiDS-1000 catalogue: Redshift distributions and their calibration,” *Astron. Astrophys.* **647** (2021) A124, [arXiv:2007.15635 \[astro-ph.CO\]](#).
- [96] O. H. E. Philcox and M. M. Ivanov, “BOSS DR12 full-shape cosmology: Λ CDM constraints from the large-scale galaxy power spectrum and bispectrum monopole,” *Phys. Rev. D* **105** no. 4, (2022) 043517, [arXiv:2112.04515 \[astro-ph.CO\]](#).
- [97] S.-F. Chen, M. White, J. DeRose, and N. Kokron, “Cosmological analysis of three-dimensional BOSS galaxy clustering and Planck CMB lensing cross correlations via Lagrangian perturbation theory,” *JCAP* **07** no. 07, (2022) 041, [arXiv:2204.10392 \[astro-ph.CO\]](#).
- [98] Z. Zhai, J. L. Tinker, A. Banerjee, J. DeRose, H. Guo, Y.-Y. Mao, S. McLaughlin, K. Storey-Fisher, and R. H. Wechsler, “The Aemulus Project. V. Cosmological Constraint from Small-scale Clustering of BOSS Galaxies,” *Astrophys. J.* **948** no. 2, (2023) 99, [arXiv:2203.08999 \[astro-ph.CO\]](#).
- [99] **DES** Collaboration, T. M. C. Abbott *et al.*, “Dark Energy Survey Year 3 results: Cosmological constraints from galaxy clustering and weak lensing,” *Phys. Rev. D* **105** no. 2, (2022) 023520, [arXiv:2105.13549 \[astro-ph.CO\]](#).
- [100] J. Lesgourgues, “The Cosmic Linear Anisotropy Solving System (CLASS) I: Overview,” *arXiv e-prints* (Apr., 2011) , [arXiv:1104.2932 \[astro-ph.CO\]](#).
- [101] D. Blas, J. Lesgourgues, and T. Tram, “The Cosmic Linear Anisotropy Solving System (CLASS). Part II: Approximation schemes,” *JCAP* **2011** no. 7, (July, 2011) 034, [arXiv:1104.2933 \[astro-ph.CO\]](#).
- [102] T. Brinckmann and J. Lesgourgues, “MontePython 3: boosted MCMC sampler and other features,” [arXiv:1804.07261 \[astro-ph.CO\]](#).
- [103] E. Ripamonti, M. Mapelli, and A. Ferrara, “Intergalactic medium heating by dark matter,” *Mon. Not. Roy. Astron. Soc.* **374** (2007) 1067–1077, [arXiv:astro-ph/0606482](#).
- [104] X.-L. Chen and M. Kamionkowski, “Particle decays during the cosmic dark ages,” *Phys. Rev. D* **70** (2004) 043502, [arXiv:astro-ph/0310473](#).

- [105] G. Hutsi, J. Chluba, A. Hektor, and M. Raidal, “WMAP7 and future CMB constraints on annihilating dark matter: implications on GeV-scale WIMPs,” *Astron. Astrophys.* **535** (2011) A26, [arXiv:1103.2766 \[astro-ph.CO\]](#).
- [106] S. Galli, T. R. Slatyer, M. Valdes, and F. Iocco, “Systematic Uncertainties In Constraining Dark Matter Annihilation From The Cosmic Microwave Background,” *Phys. Rev. D* **88** (2013) 063502, [arXiv:1306.0563 \[astro-ph.CO\]](#).
- [107] X.-L. Chen and M. Kamionkowski, “Particle decays during the cosmic dark ages,” *Phys. Rev. D* **70** 043502, [arXiv:astro-ph/0310473](#).
- [108] J. M. Shull and M. E. van Steenberg, “X-ray secondary heating and ionization in quasar emission-line clouds,” *Astrophysical Journal* **298** (Nov., 1985) 268–274.
- [109] M. Valdes and A. Ferrara, “The Energy Cascade from Warm Dark Matter Decays,” *Mon. Not. Roy. Astron. Soc.* **387** (2008) 8, [arXiv:0803.0370 \[astro-ph\]](#).
- [110] C. Evoli, M. Valdes, A. Ferrara, and N. Yoshida, “Energy deposition by weakly interacting massive particles: a comprehensive study,” *Mon. Not. Roy. Astron. Soc.* **422** (2012) 420–433.
- [111] P. J. E. Peebles, “Recombination of the Primeval Plasma,” *Astrophys. J.* **153** (1968) 1.
- [112] C. Evoli, S. Pandolfi, and A. Ferrara, “CMB constraints on light dark matter candidates,” *Mon. Not. Roy. Astron. Soc.* **433** (2013) 1736, [arXiv:1210.6845 \[astro-ph.CO\]](#).
- [113] J. Chluba and R. A. Sunyaev, “Induced two-photon decay of the 2s level and the rate of cosmological hydrogen recombination,” *Astron. Astrophys.* **446** (2006) 39–42, [arXiv:astro-ph/0508144](#).
- [114] **Planck** Collaboration, N. Aghanim *et al.*, “Planck 2018 results. V. CMB power spectra and likelihoods,” *Astron. Astrophys.* **641** (2020) A5, [arXiv:1907.12875 \[astro-ph.CO\]](#).
- [115] K. Sigurdson, M. Doran, A. Kurylov, R. R. Caldwell, and M. Kamionkowski, “Dark-matter electric and magnetic dipole moments,” *Phys. Rev. D* **70** (2004) 083501, [arXiv:astro-ph/0406355 \[astro-ph\]](#).
- [116] M. A. Buen-Abad, R. Essig, D. McKeen, and Y.-M. Zhong, “Cosmological constraints on dark matter interactions with ordinary matter,” *Phys. Rept.* **961** (2022) 1–35, [arXiv:2107.12377 \[astro-ph.CO\]](#).
- [117] Y. Ali-Haïmoud, “Boltzmann-Fokker-Planck formalism for dark-matter–baryon scattering,” *Phys. Rev. D* **99** no. 2, (2019) 023523, [arXiv:1811.09903 \[astro-ph.CO\]](#).
- [118] S. L. Dubovsky and D. S. Gorbunov, “Small second acoustic peak from interacting cold dark matter?,” *Phys. Rev. D* **64** (2001) 123503, [arXiv:astro-ph/0103122](#).
- [119] S. L. Dubovsky, D. S. Gorbunov, and G. I. Rubtsov, “Narrowing the window for millicharged particles by CMB anisotropy,” *JETP Lett.* **79** (2004) 1–5, [arXiv:hep-ph/0311189](#).
- [120] A. D. Dolgov, S. L. Dubovsky, G. I. Rubtsov, and I. I. Tkachev, “Constraints on millicharged particles from Planck data,” *Phys. Rev. D* **88** no. 11, (2013) 117701, [arXiv:1310.2376 \[hep-ph\]](#).
- [121] C.-P. Ma and E. Bertschinger, “Cosmological perturbation theory in the synchronous and conformal Newtonian gauges,” *Astrophys. J.* **455** (1995) 7–25, [arXiv:astro-ph/9506072 \[astro-ph\]](#).
- [122] D. Tseliakhovich and C. Hirata, “Relative velocity of dark matter and baryonic fluids and the formation of the first structures,” *Phys. Rev. D* **82** (Oct, 2010) 083520, [arXiv:1005.2416 \[astro-ph.CO\]](#).
- [123] M. Beltran, D. Hooper, E. W. Kolb, and Z. C. Krusberg, “Deducing the nature of dark matter from direct and indirect detection experiments in the absence of collider signatures of new physics,” *Phys. Rev. D* **80** (2009) 043509, [arXiv:0808.3384 \[hep-ph\]](#).

- [124] J. Kumar and D. Marfatia, “Matrix element analyses of dark matter scattering and annihilation,” *Phys. Rev. D* **88** no. 1, (2013) 014035, [arXiv:1305.1611 \[hep-ph\]](#).
- [125] J. Brod, A. Gootjes-Dreesbach, M. Tamaro, and J. Zupan, “Effective Field Theory for Dark Matter Direct Detection up to Dimension Seven,” *JHEP* **10** (2018) 065, [arXiv:1710.10218 \[hep-ph\]](#).
- [126] J.-H. Liang, Y. Liao, X.-D. Ma, and H.-L. Wang, “A systematic investigation on dark matter-electron scattering in effective field theories,” *JHEP* **07** (2024) 279, [arXiv:2406.10912 \[hep-ph\]](#).
- [127] X.-l. Chen, S. Hannestad, and R. J. Scherrer, “Cosmic microwave background and large scale structure limits on the interaction between dark matter and baryons,” *Phys. Rev. D* **65** (2002) 123515, [arXiv:astro-ph/0202496](#).
- [128] W. Hu, “Lecture Notes on CMB Theory: From Nucleosynthesis to Recombination,” [arXiv:0802.3688 \[astro-ph\]](#).
- [129] S. D. McDermott, H.-B. Yu, and K. M. Zurek, “Turning off the Lights: How Dark is Dark Matter?,” *Phys. Rev. D* **83** (2011) 063509, [arXiv:1011.2907 \[hep-ph\]](#).
- [130] M. A. Buen-Abad, R. Essig, D. McKeen, and Y.-M. Zhong, “Cosmological constraints on dark matter interactions with ordinary matter,” *Phys. Rept.* **961** (2022) 1–35, [arXiv:2107.12377 \[astro-ph.CO\]](#).
- [131] **DES** Collaboration, A. Amon *et al.*, “Dark Energy Survey Year 3 results: Cosmology from cosmic shear and robustness to data calibration,” *Phys. Rev. D* **105** no. 2, (2022) 023514, [arXiv:2105.13543 \[astro-ph.CO\]](#).
- [132] J. L. v. d. Busch *et al.*, “KiDS-1000: Cosmic shear with enhanced redshift calibration,” *Astron. Astrophys.* **664** (2022) A170, [arXiv:2204.02396 \[astro-ph.CO\]](#).
- [133] P. Zhang, G. D’Amico, L. Senatore, C. Zhao, and Y. Cai, “BOSS Correlation Function analysis from the Effective Field Theory of Large-Scale Structure,” *JCAP* **02** no. 02, (2022) 036, [arXiv:2110.07539 \[astro-ph.CO\]](#).
- [134] **Planck** Collaboration, P. A. R. Ade *et al.*, “Planck 2015 results. XX. Constraints on inflation,” *Astron. Astrophys.* **594** (2016) A20, [arXiv:1502.02114 \[astro-ph.CO\]](#).
- [135] **ACT** Collaboration, S. Aiola *et al.*, “The Atacama Cosmology Telescope: DR4 Maps and Cosmological Parameters,” *JCAP* **12** (2020) 047, [arXiv:2007.07288 \[astro-ph.CO\]](#).
- [136] W. L. K. Wu *et al.*, “A Measurement of the Cosmic Microwave Background Lensing Potential and Power Spectrum from 500 deg² of SPTpol Temperature and Polarization Data,” *Astrophys. J.* **884** (2019) 70, [arXiv:1905.05777 \[astro-ph.CO\]](#).
- [137] **XENON10** Collaboration, J. Angle *et al.*, “A search for light dark matter in XENON10 data,” *Phys. Rev. Lett.* **107** (2011) 051301, [arXiv:1104.3088 \[astro-ph.CO\]](#). [Erratum: *Phys.Rev.Lett.* 110, 249901 (2013)].
- [138] **DarkSide** Collaboration, P. Agnes *et al.*, “Low-Mass Dark Matter Search with the DarkSide-50 Experiment,” *Phys. Rev. Lett.* **121** no. 8, (2018) 081307, [arXiv:1802.06994 \[astro-ph.HE\]](#).
- [139] **XENON** Collaboration, E. Aprile *et al.*, “Light Dark Matter Search with Ionization Signals in XENON1T,” *Phys. Rev. Lett.* **123** no. 25, (2019) 251801, [arXiv:1907.11485 \[hep-ex\]](#).
- [140] **XENON** Collaboration, E. Aprile *et al.*, “Emission of single and few electrons in XENON1T and limits on light dark matter,” *Phys. Rev. D* **106** no. 2, (2022) 022001, [arXiv:2112.12116 \[hep-ex\]](#). [Erratum: *Phys.Rev.D* 110, 109903 (2024)].
- [141] **PandaX-II** Collaboration, C. Cheng *et al.*, “Search for Light Dark Matter-Electron

- Scatterings in the PandaX-II Experiment,” *Phys. Rev. Lett.* **126** no. 21, (2021) 211803, [arXiv:2101.07479 \[hep-ex\]](#).
- [142] **DarkSide** Collaboration, P. Agnes *et al.*, “Search for Dark Matter Particle Interactions with Electron Final States with DarkSide-50,” *Phys. Rev. Lett.* **130** no. 10, (2023) 101002, [arXiv:2207.11968 \[hep-ex\]](#).
- [143] **SENSEI** Collaboration, P. Adari *et al.*, “First Direct-Detection Results on Sub-GeV Dark Matter Using the SENSEI Detector at SNOLAB,” *Phys. Rev. Lett.* **134** no. 1, (2025) 011804, [arXiv:2312.13342 \[astro-ph.CO\]](#).
- [144] **DAMIC-M** Collaboration, I. Arnquist *et al.*, “First Constraints from DAMIC-M on Sub-GeV Dark-Matter Particles Interacting with Electrons,” *Phys. Rev. Lett.* **130** no. 17, (2023) 171003, [arXiv:2302.02372 \[hep-ex\]](#).
- [145] F.-Y. Cyr-Racine, K. Sigurdson, J. Zavala, T. Bringmann, M. Vogelsberger, and C. Pfrommer, “ETHOS—an effective theory of structure formation: From dark particle physics to the matter distribution of the Universe,” *Phys. Rev. D* **93** no. 12, (2016) 123527, [arXiv:1512.05344 \[astro-ph.CO\]](#).
- [146] M. R. Buckley, “Asymmetric Dark Matter and Effective Operators,” *Phys. Rev. D* **84** (2011) 043510, [arXiv:1104.1429 \[hep-ph\]](#).